(*16*). Conversely, TAT-conjugated liposomes were recently shown to enter acidic Lysotracker-positive compartments (*19*), and full-length TAT protein also entered acidic late endocytic structures containing the mannose 6-phosphate receptor (*20*). Indeed the ability of TAT protein to translocate to the cytosol was dependent on it reaching acidic organelles. For utilization of PTDs as cellular vectors for delivery of lysosome-fragile entities such as proteins and DNA, it is imperative that the trafficking route of these molecules downstream from the plasma membrane is delineated.

New nonviral systems for the delivery of macromolecules into hematopoietic cells are required for phenotype manipulation of precursor stem cells and for improved therapy against drug resistant leukemias (*21*). Green Fluorescent Protein conjugated to a TAT derivative and an alternate PTD were both found to be internalized into a number of primary hematopoietic cells, suggesting that this may be a promising avenue for delivery of macromolecular entities into these cells (*22*). In addition, overcoming multidrug resistance in leukemia cells via conjugation of a PTD to the anthracycline doxorubicin has also been demonstrated (*23*).

Overall it is clear that a greater understanding of PTD trafficking is a key requisite for extending their potential use in therapy. To address this we investigated and compared the intracellular traffic of fluorescent conjugates of TAT and octaarginine (R8) peptides in human leukemia KG1a-CD34$^+$ and K562-CD34$^-$ cells, that serve as models for primary hematopoietic stem cells and myeloid leukemia. In this report we show that despite the fact that the two cell lines have major differences in their interaction with PTDs at different temperatures and distinct organization of their endocytic pathways, they both deliver TAT-peptide and R8 to lysosomes. We extend these studies to adherent cells and demonstrate that lysosomal sequestration may be a common cellular fate following endocytic capture. Finally, the significance of these findings with respect to their potential as drug delivery vectors is discussed.

EXPERIMENTAL PROCEDURES

Reagents. Wortmannin, Cytochalasin D (CytD), 5-(*N*-ethyl-*N*-isopropyl)amiloride (EIPA), brefeldin A (BFA), nocodazole, and porcine intestinal mucosa heparin were from Sigma. Sheep anti-TGN46 was from Serotec, Oxford, UK, mouse anti-Lamp-II and anti-EEA1 antibodies were from DSHB, and BD Biosciences, Oxford, UK, respectively. Texas Red (TxR) (10000 Mw) and tetramethylrhodamine (TMR)−dextran conjugates, lysine fixable TxR-dextran (10000 Mw), TxR-transferrin (TxR-Tf), and Alexa594 and 488 labeled anti-sheep and anti-mouse antibodies were from Molecular Probes, Paisley, UK. Mounting medium containing 1.5 μg/mL 4′,6-diamidino-2-phenylindole dihydrochloride (DAPI) was from Vector Laboratories, Burlingame, CA. All cell culture reagents were from Invitrogen, Paisley, UK.

Peptide Synthesis. All the peptides used in this study were chemically synthesized as described below, and their structures are shown in Figure 1. All peptides were purified by high performance liquid chromatography (HPLC), and the molecular masses were confirmed by matrix-assisted laser desorption ionization time-of-flight mass spectrometry (MALDI-TOFMS).

TxR-labeled R8 peptide: The peptide chain was constructed by Fmoc (= 9-fluorenylmethyloxycarbonyl)-solid-phase peptide synthesis on a Rink amide resin (*24*) as previously reported (*25, 26*). After removal of the N-terminal Fmoc group, the N-terminus of the peptide resin was fluorescently labeled by treatment with TxR-X succinimidyl ester mixed isomer (Molecular Probes) (*27*). The fluorescently labeled peptide resins were then treated with trifluoroacetic acid (TFA)−ethanedithiol (EDT) (95:5) at 25 °C for 2 h to yield TxR−(Arg)$_8$-amide.

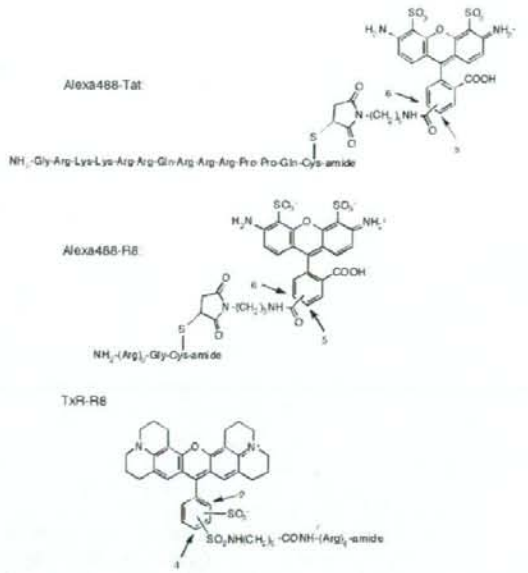

Figure 1. Structures of the fluorescently labeled peptides. In Alexa488-Tat and -R8, the linker is connected to the phenyl moiety at position 5 or 6, and in TxR-R8 the (sulfonamide) linker is connected at position 2 or 4 of the phenyl ring.

MALDI-TOFMS: 1969.0 [calcd for (M + H)$^+$: 1969.4]. Retention time in HPLC was 17.4 min [Column: Cosmosil 5C4-AR-300 (4.6 × 150 mm); Gradient: 5−95% B in A (A = H_2O containing 0.1% CF_3COOH, B = CH_3CN containing 0.1% CF_3COOH) over 40 min; Flow: 1 mL/min; Detection: 215 nm].

Alexa-labeled peptides (Alexa488-TAT or Alexa488-R8): The peptide segments bearing extra cysteine or glycylcysteine residues at the C-terminus of the arginine segments were prepared by Fmoc-solid-phase peptide synthesis followed by the treatment in TFA−EDT and HPLC purification. Peptides were then treated with Alexa488 C_5 maleimide sodium salt (Molecular Probes) and purified by HPLC. The sequences of the synthesized peptides are Alexa488-TAT, NH_2-Gly-Arg-Lys-Lys-Arg-Arg-Gln-Arg-Arg-Arg-Pro-Pro-Gln-Cys(Alexa)-amide; Alexa488-R8, NH_2-(Arg)8-Gly-Cys(Alexa)-amide. MALDI-TOFMS; Alexa-TAT: 2521.1 [calcd for (M + H)$^+$: 2520.9]; Alexa-R8: 2126.81 [calcd for (M + H)$^+$: 2126.4]. Retention time in HPLC: 3.1 min (Alexa488-Tat) and 3.0 min (Alexa488-R8) [Column: Chromolith Performance (4.6 × 100 mm); Gradient: 5−85% B in A (A = H_2O containing 0.1% CF_3COOH, B = CH_3CN containing 0.1% CF_3COOH) over 10 min; Flow: 4 mL/min; Detection: 215 nm].

Cell Culture. Cells were maintained at 37 °C in a humidified 5% CO_2 incubator. K562 cells, a gift from Dr. Paul Brennan (Cardiff University), and KG1a cells (ECACC 91030101) were maintained at a confluency of (0.5−5) × 10^6 in RPMI 1640 media supplemented with 10% fetal calf serum (FCS), 100 IU/mL penicillin, and 100μg/mL streptomycin. HeLa cells were maintained in D-MEM supplemented with 10% FCS, 100 IU/mL penicillin, and 100μg/mL streptomycin.

Fluorescence Microscopy. Images were acquired on either a Leica DMIRB inverted fluorescent microscope or a Leica SP2 RS confocal laser rapid scanning microscope as previously described (*28*). For double label live cell imaging, cells were loaded with endocytic markers or peptides as described below and washed in imaging medium, and aliquots were placed in eight-chambered coverglass slides (Nalgene Nunc International) prior to confocal microscopy. For this the cells were maintained at 37 °C/5% CO_2 and imaged at between 1.0 and 3.0 frames

s^{-1} using an UltraView RS real-time confocal system (Perkin-Elmer) consisting of a Zeiss Axiovert 200 microscope equipped with a 1.3 NA PlanFluar 100× objective and a three line Argon−Krypton laser. Images were merged and stacked using NIH ImageJ version 1.33 software, and the background fluorescence was removed using the 'despeckle' filter.

Transferrin Labeling in K562 and KG1a Cells. Cells (5×10^5) were incubated with 25 ng/mL TxR-Tf in 0.5 mL serum free media for 1 min at 37 °C prior to addition of 1 mL of ice cold 10 mM phosphate buffered serum, pH 7.4 (PBS). The cells were centrifuged for 1 min (1500g) at 4 °C and washed 4× in ice cold PBS containing 0.2% w/v BSA. The final cell pellet was resuspended in 70 μL of imaging medium (DMEM lacking Phenol Red containing 25 mM HEPES pH 7.4) and analyzed within 2 min by fluorescence microscopy.

For colocalization experiments of peptides with TxR-Tf, K562 cells were incubated with 3 μM Alexa488-TAT for 90 min prior to a further incubation in peptide free medium for 120 min. The cells were washed and incubated for 6 min at 37 °C with 50 ng/mL TxR-Tf in serum free medium containing 25 mM HEPES, pH 7.4. The cells were washed 3× in PBS and 1× in imaging medium prior to analysis by confocal microscopy.

Dextran Uptake and Distribution in K562 and KG1a Cells. For initial localization studies, 5×10^5 cells in 0.5 mL of complete medium were incubated for 60 min at 37 °C with 0.5 mg/mL TMR-dextran (*29*). The cells were then washed 4× in PBS and analyzed by fluorescence microscopy in imaging medium as described.

Peptide Uptake and Distribution in K562 and KG1a Cells. Cells (5×10^5) in 0.5 mL complete medium were incubated for 60 min at 37 °C with 1μM TxR-R8, Alexa488-R8 or 3μM Alexa-488 TAT. The cells were then washed 4× in PBS and analyzed by fluorescence microscopy in imaging medium as described. For BFA experiments cells were allowed to internalize the fluorescent peptides as above, washed and then incubated for 30 min at 37 °C in 5μg/mL BFA or control diluent. The cells were then analyzed by fluorescence microscopy.

Dextran and Peptide Uptake and Distribution in K562 and KG1a Cells. Cells (5×10^5) were incubated with TxR-dextran for 120 min as described, and the label was then chased into lysosomes via a further incubation in dextran-free medium for 300 min (chase) (*29*). At 120 and 180 min chase, the cells were washed to remove any recycled label. At the end of the chase period, the cells were washed and incubated with either 3 μM Alexa488-TAT or 1 μM Alexa488-R8 in complete medium for 60 min at 37 °C. The cells were washed 3× in PBS and analyzed by live-cell confocal microscopy as previously described. For analysis of the effects of pharmacological inhibitors of endocytic processes, dextran was internalized and chased as described prior to preincubation for 15 min at 37 °C with either 50 μM CytD or 10 μM nocodazole. In the continued presence of the drug the cells were then incubated at 37 °C for 60 min with Alexa488 peptides as described. The inhibitors were also present during the subsequent washing processes and confocal imaging.

Dextran and Peptide Uptake and Distribution in HeLa Cells. HeLa cells (1.2×10^5) were seeded on glass bottomed 35 mm culture dishes (MatTek Corporation, Ashland) and allowed to adhere for 15 h. The cells were then incubated for 120 min at 37 °C in complete medium containing 0.5 mg/mL TxR-dextran (*29*). Cells were washed and incubated for 240 min in complete medium prior to a further 60 min incubation in complete medium containing 2 μM Alexa488-TAT. The cells were washed and analyzed by confocal microscopy at 37 °C/5% CO_2.

Quantification of Alexa488-peptide Uptake by Flow Cytometry. K562 cells (5×10^5) were washed 2× in PBS and resuspended in 200 μL of RPMI 1640 medium supplemented with 10% FCS and containing either 10 μM EIPA, 150 nM wortmannin, 10 μM nocodazole, or their respective diluents. The cells were incubated for 15 min at 37 °C prior to the addition of 3 μM Alexa488-Tat or 1 μM Alexa488-R8 and incubated for 60 min in the continued presence of the drug. Equivalent aliquots of cells were precooled to 4 °C and incubated with the peptides on ice. Following all peptide incubations, the cells were washed 3× in PBS prior to incubation in 0.25 g/L trypsin for 5 min at 37 °C. Trypsinization was stopped by addition of an excess of ice cold PBS and cells were washed 2× in PBS, 3× in 15 μg/mL heparin/PBS and a further two washes in ice cold PBS. The cells were finally resuspended in 200 μL of PBS, and fluorescence was measured immediately on a Becton Dickinson FACSCalibur analyzer. The fluorescence of 10000 viable cells was acquired. Each experiment was performed at least two times, each condition was analyzed in triplicate, and statistical significance was assessed by analysis of variance (ANOVA), followed by Dunnett's multiple comparison between means.

Immunostaining. K562/KG1a cells: 1×10^6 cells were washed in PBS, fixed in 2% paraformaldehyde (PFA) in PBS for 15 min, and washed, and aliquots were transferred to wells on a multispot microscope slide (Hendley, UK). For some experiments, the lysosomes were preloaded as described with lysine fixable TxR-dextran prior to fixing. The cells were dried on to the slide and permeabilized with 0.1% Triton X-100 in PBS (for TGN46, EEA1 labeling) or acetone (for Lamp-II labeling) before blocking nonspecific binding sites with 10% v/v fetal calf serum/PBS for 10 min. Cells were then incubated with anti-TGN46, Lamp-II or EEA1 antibodies for 30 min in a humidified box at 37 °C. Cells were washed 3× with 0.1% Triton X-100 in PBS (TGN46, EEA1) or PBS alone (Lamp-II) and then incubated for 30 min with Alexa594 or Alexa488 conjugated secondary antibodies. The cells were washed as before and overlaid with 5 μL of mounting medium containing DAPI. The wells were covered with a coverslip and sealed with nail polish prior to analysis by confocal fluorescence microscopy. To test the effect of BFA on TGN46 labeling, cells were incubated with 5 μg/mL BFA in complete medium for 30 min at 37 °C prior to fixation and immunolabeling. HeLa cells: BFA treated (as above) or control cells were washed in PBS and processed for immunofluorescence microscopy as previously described (*28*) and labeled with antibodies against TGN46 or Lamp-II.

RESULTS

Distribution of TAT and R8 in Hematopoietic Cells. Numerous recent reports have provided strong evidence that endocytosis is a major entry route for PTDs such as TAT and penetratin. The ability to monitor and resolve traffic downstream of the plasma membrane in adherent cell culture models, using fluorescence microscopy, is hampered by the extensive binding of these peptides to the plasma membrane and tissue culture surfaces. We therefore investigated the uptake of two fluorescently conjugated PTD peptides TAT and R8 in nonadherent leukemia cell lines K562 and KG1a. For this, both cell lines were initially incubated with 3 μM Alexa488-TAT for 120 min at 37 °C, and after washing, the cellular localization of the peptide was analyzed by fluorescence microscopy. As fixing has been shown to cause major artifacts in the intracellular localization of PTDs, all fluorescence microscopy studies, unless otherwise specified, were performed in live cells. Figure 2 shows that although both cell lines contained internalized peptide, there were major differences in its subcellular distribution. In K562

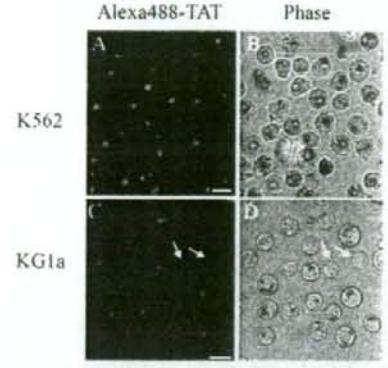

Figure 2. Distribution of Alexa488-TAT in myeloid leukemia cell lines. K562 (A,B) and KG1a (C,D) cells were incubated with 3μM Alexa488-TAT for 120 min at 37 °C prior to washing and analysis by fluorescence and bright field microscopy. Arrows denote KG1a cells containing very low amounts of fluorescence. Scale bars 25 μm.

cells, labeling was enriched in the perinuclear region; however, in KG1a cells, the peptide was predominantly localized in small disperse cytoplasmic vesicular structures. The majority of the cells contained labeled structures, but within each cell line there was variation in the intensity of labeling. Under these conditions, we could not detect significant nuclear or cytosolic labeling.

In view of these data and the paucity of information on the subcellular organization of organelles at specific locations on the endocytic pathway in these cell lines, especially KG1a, we labeled distinct endocytic structures of both cell lines with fluorescent probes whose intracellular fate following endocytic capture is well defined. Transferrin enters cells via clathrin-coated vesicles after binding to the transferrin receptor and traffics through early and recycling endosomes en route for return to the plasma membrane (*30*). In this study we generally define early endosomes as organelles containing internalized probe after 0−10 min of uptake, late endosomes (10−30 min), lysosomes (30+ min) (*30, 31*). Plasma membrane derived vesicles and early endosomes were labeled in both cell lines by internalizing TxR-Tf for only 1 min, followed by immediate microscopic analysis. In both cell lines the plasma membrane was labeled, in addition to distinct punctate structures (Figure 3A−D). Endocytosis of dextran is also well characterized in terms of its fluid phase uptake into early endosomes, through late endosomes, and finally to lysosomes (*32, 33*). K562 and KG1a cells were incubated with TMR-dextran for 60 min, thus allowing labeling of early and late endosomal compartments. Similar to observations with Alexa488-TAT (Figure 2), dextran-labeled vesicles were strongly enriched in the perinuclear region of K562 cells (Figure 3E,F); however, in KG1a cells the dextran-labeled structures were distributed throughout the peripheral cytoplasm (Figure 3G,H). The subcellular distribution profiles of fluorescent TAT and R8 after internalization at 37 °C for 60 min were then compared. As shown in Figure 3I−P, the distribution patterns of both peptides were similar to each other in each respective cell line, indicative of trafficking to the same structures. We observed minimal plasma membrane labeling of the peptides at 37 °C, and the labeling was predominantly confined to internal punctate structures. Cells treated with peptides had normal morphologies, and using an apoptosis assay utilizing YO−PRO-1 and propidium iodide dyes followed by flow cytometry, we found no increase in permeability to these agents in either cell line when they were incubated with 3 μM TAT or R8 for up to 4 h (data not shown).

Effect of Endocytosis Inhibitors on Peptide Uptake. The contribution of endocytosis to peptide uptake was then investigated by flow cytometry after treating cells with pharmacological agents that disrupt endocytic processes. K562 cells were pretreated with wortmannin, nocodazole, or EIPA prior to addition of the peptides for 60 min in the continued presence of the drug. The PI 3-kinase inhibitor wortmannin affects uptake at the plasma membrane and several downstream trafficking events (*34, 35*), nocodazole depolymerizes microtubules and also affects numerous endocytic processes including uptake at the plasma membrane and delivery through the endocytic pathway (*36*), while the amiloride analogue EIPA has been shown to inhibit macropinocytosis (*37*). We observed, in most cases, similar effects on uptake of both TAT and R8 in the presence of these agents (Figure 4A). The addition of 10 μM EIPA resulted in only a minimal decrease in peptide uptake, with only the uptake of R8 being statistically significant. We also performed experiments at higher EIPA concentrations, but toxicity issues possibly related to increases in intracellular pH and apoptosis (*38*) predominated over uptake effects (data not shown). Microtubule depolymerization inhibited uptake of both peptides by ~30%, and cells treated with wortmannin had significantly lower (~50%) fluorescence. The effect of incubating cells with CytD and methyl-β-cyclodextrin to compare the requirements of the actin cytoskeleton and lipid rafts, respectively, on peptide uptake (*39*) was also investigated. However, even the relatively mild treatments that we used for reducing plasma membrane labeling following internalization led to a significant enhancement of minimal effects of CytD that were observed in the absence of trypsinization, and in the case of methyl-β-cyclodextrin, trypsinization led to significant increases in dead cells identified via trypan blue staining.[2]

Finally to determine whether peptide internalization in these cells is an energy-dependent process, the effects of reducing incubation temperature was examined. Incubating K562 cells with peptides on ice resulted in a >88% decrease in fluorescence compared to cells incubated with the peptide at 37 °C (Figure 4A). In KG1a cells, however, the fluorescence of cells incubated with peptide on ice was often equal to or even higher than those incubated at 37 °C. Using flow cytometry, we compared cell numbers versus fluorescence intensity profiles of K562 and KG1a cells after incubation with both peptides at 4 °C and 37 °C and for 5 and 60 min (Figure 4B). After 5 min there was a clear difference between the 37 °C and 4 °C profiles for both peptides in the two cell lines, with the expected increased fluorescence at the higher temperature. However, after 60 min there was significant fluorescence in KG1a cells incubated at 4 °C, and the mean fluorescence of a large population of these cells was often higher than those incubated at 37 °C. These experiments were performed three times with two batches of peptides, and although there was much higher variation in cell-associated fluorescence at 4 °C, the value was always at least 50% of the control 37 °C value and in some cases was 2-fold higher.

Peptide distribution in KG1a cells after incubation at the two temperatures was then analyzed by fluorescence microscopy. The left panel of Figure 4C shows that after incubating the cells with R8 peptide on ice for 60 min followed by trypsinization and heparin washes, cell-associated fluorescence was still clearly evident, but rather than being located in distinct punctate structures, as previously observed (see Figure 3O), the peptide diffusely labeled and outlined the entire cell. Although the staining pattern was the same in all cells, we observed a high degree of heterogeneity with respect to fluorescence intensity, as some cells were very bright and others had much lower fluorescence. This heterogeneity is clearly observed by comparing the fluorescence of the three cells in Figure 4C. In cells incubated with the peptide at 37 °C, and then treated with trypsin and heparin, the peptide was predominantly localized in

[2] A.T.J., personal communication.

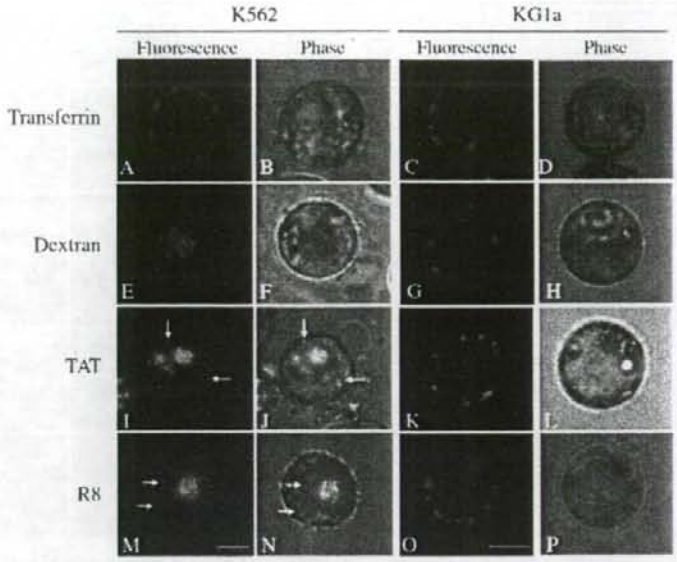

Figure 3. Comparison of cellular localization of endocytic probes with TAT and R8. (A−H) K562 (A,B, E,F) and KG1a (C,D, G,H) cells were incubated with Texas-red transferrin for 1 min (A−D) or TMR-dextran for 60 min (E−H) prior to washing and analysis by fluorescence and bright field microscopy. (I−P) K562 (I,J, M,N) and KG1a (K,L, O,P) cells were incubated with 3 μM Alexa488-TAT (I−L), 1 μM Alexa488-R8 (M,N) or 1 μM TxR-R8 (O,P) for 60 min prior to washing and analysis by fluorescence and bright field microscopy. Arrows show peptide-positive vesicles peripheral to the perinuclear structures. Scale bars 10 μm.

vesicular structures, similar to that seen in untreated cells. Increasing the trypsin concentration 2-fold, the length of the heparin washes to 5 min and the heparin concentration to 50 μg/mL did not significantly diminish the amount of peptide bound to the cells (data not shown).

Identification of Peptide Labeled Structures. Previous analysis of the intracellular traffic of TAT peptide in HeLa cells suggested that it bypasses late endosomal and lysosomal structures and traffics to the Golgi (*14*). We therefore further characterized the peptide labeled vesicles, initially in leukemia cells, and investigated whether they were morphologically sensitive to agents that disrupt membrane traffic on endocytic and secretory pathways. Cells treated with the phosphoinositide 3-kinase inhibitor wortmannin are characterized by the appearance of swollen vacuole-like endosomes (*35, 40*). This is primarily due to inhibition of hVPS34 protein that is required for formation of phosphatilylinositol 3-phosphate on endosome membranes and vesicles within the lumen of the endosome (*41*). We therefore analyzed the localization pattern of Alexa488-TAT after uptake into cells pretreated with 150 nM wortmannin. Only minor wortmannin effects were observed in K562 cells (Figure 5A−D), but this was difficult to visualize, as the peptide, despite the presence of the drug, still accumulated in the perinuclear region. In KG1a cells a dramatic wortmannin-induced redistribution of both TxR-R8 and Alexa488-TAT into enlarged vacuole-like structures was observed (Figure 5E−J).

To investigate whether TAT and R8 peptides traffic to the Golgi, cells were incubated with either Alexa488-TAT or -R8 for 120 min and then incubated for 60 min in the presence of the Golgi-disrupting agent brefeldin A (BFA) (*42*). Figure 5A-D shows that in K562 cells, there was no visible difference in the Alexa488-TAT labeling pattern in the presence or absence of BFA. This experiment was also performed in KG1a cells, and they yielded the same results (data not shown). To analyze the localization of the Golgi in these cell lines and to assess the activity of BFA, cells incubated in the absence or presence of the drug were fixed and immunolabeled with antibodies against the *trans*-Golgi marker TGN46. Previous studies have shown that BFA collapses the *cis/medial* Golgi cisterna into the endoplasmic reticulum and causes the relocation of the *trans*-Golgi network (TGN) to a compact centrosomal location with some diffuse staining of the cytoplasm (*43−45*). In untreated K562 cells, TGN46 labeling was almost exclusively confined to a perinuclear region that was, as previously shown, conspicuous in cells incubated with the fluorescent peptides (Figure 6E,F). However, on treatment with BFA, a relocation of a significant fraction of the protein to diffuse cytoplasmic vesicles and reticular networks was observed (Figure 6G,H). The Golgi was also prominent in untreated KG1a cells (Figure 6I,J) and unlike in K562 cells which harbor both TGN46, TAT, and R8 in a perinuclear region, the TGN distribution in KG1a cells was markedly different to that of the internalized peptides (Figure 3O,P). TGN46 labeling in KG1a cells was also markedly sensitive to BFA (Figure 6K,L). Together, the data strongly suggest that the major fraction of internalized TAT and R8 does not traffic to the Golgi.

These data prompted us to design further experiments to characterize the organelles enriched with endocytosed TAT and R8. K562 cells were incubated with TxR-dextran for 120 min prior to washing and a further incubation in dextran-free medium for 5 h to allow the label to empty from early endosomes and traffic (chase) to lysosomal compartments (*29, 33, 46, 47*). By this method, the label would be depleted from early and late endosomes, and the potential re-entry of recycled label was minimized by washing during the chase period. Dextran-loaded cells were then incubated for 60 min with Alexa488-TAT or -R8, and the subcellular location of both labels was analyzed by double-labeling confocal microscopy. We observed extensive colocalization of both R8 and TAT with dextran in highly motile perinuclear structures of the K562 cells (Figure 7A−C; Movie 1, Supporting Information). Some single-labeled structures were observed, possibly representing peptide that had not yet reached the dextran-loaded compartment; tubulation of TAT-labeled structures was also apparent. A similar degree of high colocalization was also observed when dextran-loaded cells were incubated with Alexa488-R8 (Figure 7D−F; Movie 2, Supporting Information).

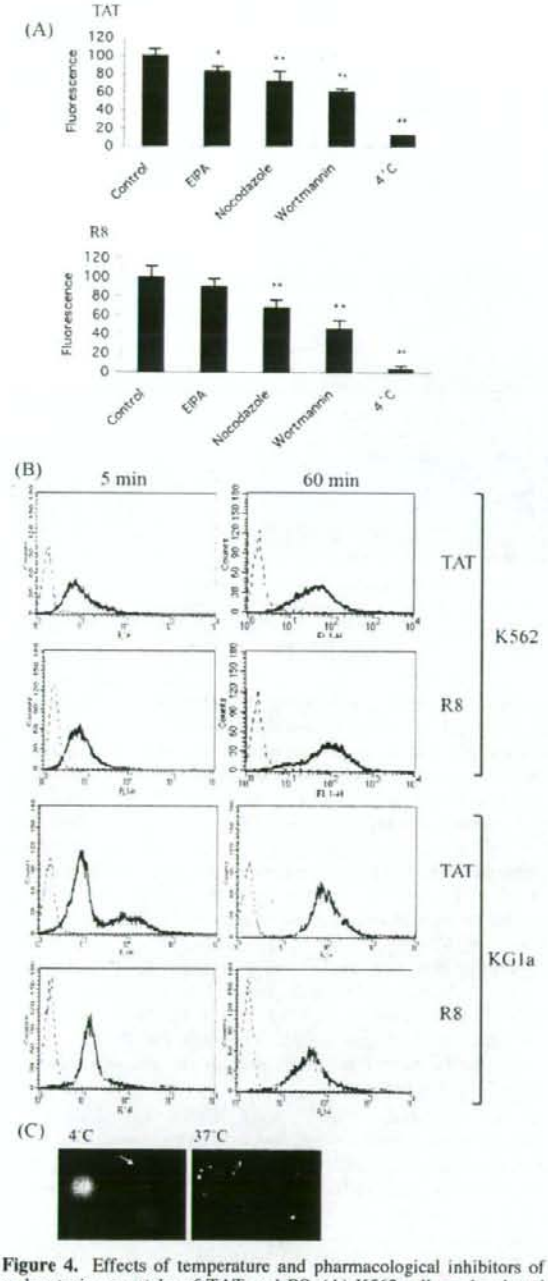

Figure 4. Effects of temperature and pharmacological inhibitors of endocytosis on uptake of TAT and R8. (A) K562 cells preincubated with diluent (control) or 10 μM EIPA, 10 μM nocodazole, and 150 nM wortmannin were incubated, in the continued presence of the drug, with 1 μM Alexa488-TAT (upper panel) or 3 μM Alexa488-R8 (lower panel) for 60 min prior to trypsin/heparin treatment and analysis by flow cytometry as described in Materials and Methods. Equivalent aliquots of cells were incubated with the peptides on ice (4 °C). (B) K562 and KG1a cells were incubated with 3 μM Alexa488-TAT or 1 μM Alexa488-R8 for either 5 or 60 min at 37 °C or 4 °C prior to trypsin/heparin treatment and analysis by flow cytometry. The number of cells (*y*-axis) is plotted against the fluorescence signal of cells (*x*-axis); 37 °C (black line), 4 °C (grey line) untreated cells dotted line. (C) KG1a cells were incubated with 1 μM Alexa488-R8 for 60 min at either 4 °C (left panel) or 37 °C (right panel) to prior to trypsin/heparin treatment and after by fluorescence microscopy. Arrow denotes cell with low fluorescence. * Statistically significant * $p < 0.05$, ** $p < 0.01$.

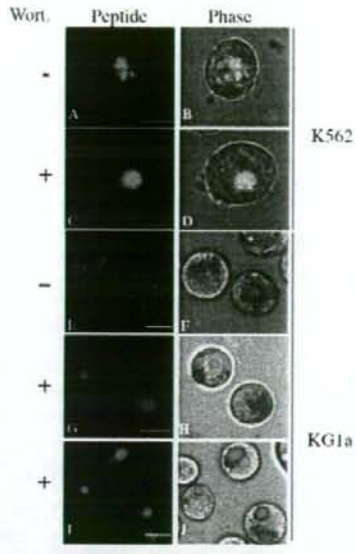

Figure 5. TAT and R8 distribution in wortmannin treated cells. K562 (A−D) or KG1a (E−J) cells were incubated for 15 min in control media (A,B, E,F) or media containing 150 nM wortmannin (C,D, G−J). The cells were then incubated with 3 μM Alexa488-TAT (A−D), 1 μM TxR-R8 (E−H) or 3 μM Alexa488-TAT (I,J) for 60 min in the continued presence of the drug or DMSO equivalent. The cells were washed and analyzed by fluorescence and bright field microscopy. Scale bars 10 μm.

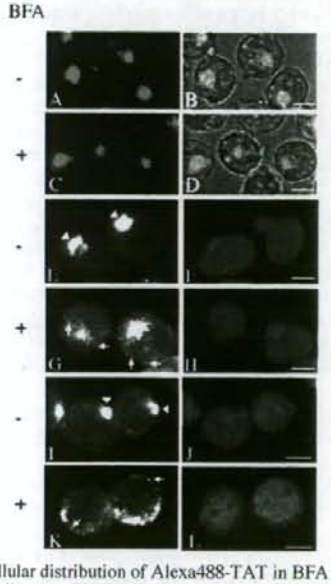

Figure 6. Cellular distribution of Alexa488-TAT in BFA treated K562 and KG1a cells. (A−D) K562 cells were incubated with 3 μM Alexa488-TAT for 60 min prior to washing and a further incubation for 30 min in control medium or medium containing (5 μg/mL) BFA. The cells were washed and analyzed by fluorescence and bright field microscopy. (E−L) K562 (E−H) or KG1a (I−L) cells were incubated in the absence or presence of 5 μg/mL BFA for 30 min prior to fixing and labeling with anti-TGN46 antibodies followed by secondary Alexa594 anti-sheep antibodies and analysis by fluorescence microscopy. Arrowheads denote compact Golgi staining in control cells, arrows denote TGN46-positive vesicles in BFA-treated cells. Scale bars 10 μm.

We then investigated whether the peptides, in a fashion similar to dextran, could be depleted from early endosomes and

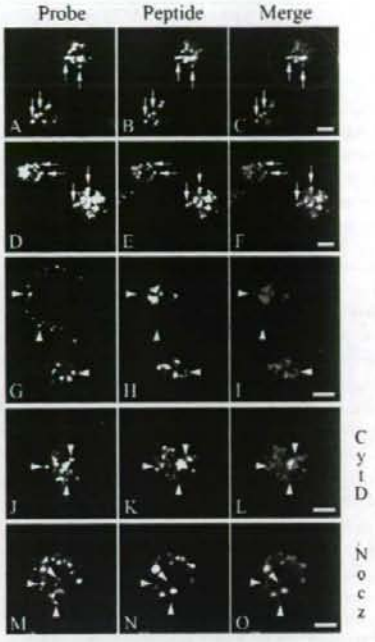

Figure 7. Colocalization of TAT and R8 with dextran in lysosomes of K562 cells. (A−F) K562 cells were incubated in the presence of TxR-dextran for 120 min and then washed and further incubated in dextran-free medium (chase) for 300 min. The cells were then allowed to internalize 3 μM Alexa488-TAT (A−C) or 1 μM Alexa488-R8 (D−F) for 60 min prior to washing and analysis by live-cell confocal microscopy. (G−I) K562 cells were allowed to internalize Alexa488-TAT for 90 min prior to washing and incubating in peptide free medium for 120 min. Cells were then incubated in 50 ng/mL TxR-Tf for 6 min prior to washing and analysis by live-cell confocal microscopy. (J−O) Cells were incubated with TxR-dextran as in A−F and following the chase period the cells were preincubated for 15 min with 50 μM CytD (J−L) or 10 μM nocodazole (M−O) and then incubated with 3 μM Alexa488-TAT in the continued presence of the drug. The cells were washed and analyzed by live-cell confocal microscopy. Arrows denote colocalization of peptide with dextran in the perinuclear region, and arrowheads denote uniquely labeled structures. The circle in C represents the plasma membrane of the cell. The data in A−O show the first frame of the accompanying movies: Movie 1 Image C, Movie 2 Image F, Movie 3 Image I, Movie 4 Image L, and Movie 5 Image O. Scale bars 10 μm.

chased into lysosomal structures. For this, K562 cells were allowed to internalize Alexa488-TAT for 120 min prior to washing and chasing the label through the endocytic pathway via a further 90 min incubation in peptide-free medium. Early endosomes were then labeled by a 6 min incubation with 50 ng/mL TxR-Tf prior to washing and live cell imaging. TxR-Tf was mainly localized to peripheral cytoplasmic structures, but interestingly in this short incubation time and during the imaging process a fraction of the ligand had traversed into a perinuclear location (Figure 7G−I; Movie 3, Supporting Information). The perinuclear staining is more prominent in the lower cell in Figure 7G; however, both peripheral and perinuclear structures were distinct from TAT-labeled structures with very little colocalization between the two labels. We next investigated whether actin disruption inhibited the delivery of TAT to dextran-labeled lysosomes. TxR-dextran was first chased into K562 lysosomes as previously described, and then the cells were preincubated with 50 μM CytD for 15 min prior to adding 3 μM Alexa488-TAT and incubating for a further 60 min in the continued presence of the drug. Figure 7J−L and Movie 4 (Supporting Information) show that there is very little colocalization of TAT

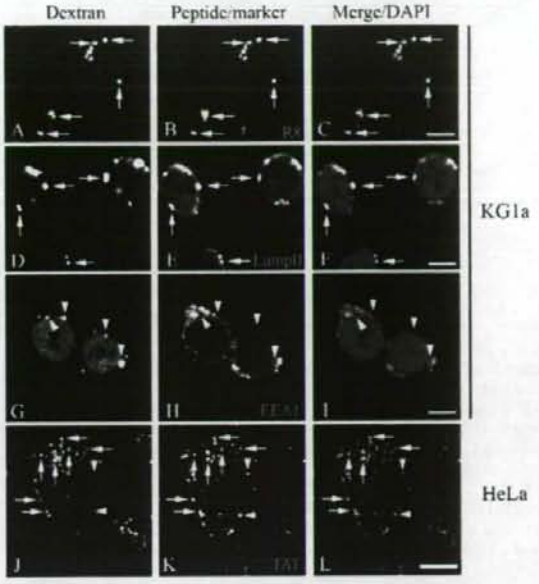

Figure 8. Colocalization of Alexa488-TAT and dextran in lysosomes of KG1a and HeLa cells. KG1a (A−I) and HeLa cells (J−L) were incubated in the presence of TxR-dextran (A−C, J−L) or (D−I) lysine fixable TxR-dextran for 120 min and then washed and further incubated in dextran-free medium (chase) for 300 min. (A−C, J−L). Cells were then incubated with 1 μM Alexa488-R8 (A−C) or 3 μM Alexa488-TAT (J−L) for 60 min prior to washing and analysis by live-cell confocal microscopy or immediately fixed and labeled with antibodies against Lamp-II (D−F) or EEA1 (G−I) and secondary Alexa488 conjugated anti-mouse antibodies and analyzed by confocal fluorescence microscopy. Arrows in A−C and J−L denote colocalization of TxR-dextran with Alexa488 peptides and arrowheads denote peptide unique structures. Arrows in D−F show colocalization of dextran with Lamp-II and arrowheads in G−I show dextran positive EEA1 negative structures. A−C, J−L show the first frame of the movies: Movie 6 Image C and Movie 7 Image L. Scale bars 10 μm.

and dextran in these cells with both probes labeling distinct vesicles. The distribution of peptide labeling was quite variable, but peptide-labeled structures were often peripheral to the lysosomes, the distribution of which were relatively unaffected by CytD. These observations strongly suggest that the traffic of TAT to lysosomes has a requirement for the actin cytoskeleton.

Lysosomes have been shown to be associated with microtubules, and loss of microtubule integrity has been shown to affect lysosome distribution, and delivery of material to late endocytic structures (*48*, *49*). We therefore used the microtubule-disrupting agent nocodazole to investigate the involvement of microtubules in peptide traffic. K562 lysosomes were labeled with dextran as described, and then Alexa488-TAT was incubated in nocodazole pretreated cells in the continued presence of the drug. There was very little colocalization of the two probes in these cells (Figure 7M−O; Movie 5, Supporting Information), and both peptide and dextran were localized in vesicular structures that were scattered throughout the cytoplasm. In these experiments nocodazole appeared to inhibit traffic of the peptide to the perinuclear region and also to dissipate the perinuclear lysosomes. The movie also demonstrates that compared to control cells there was very little overall vesicular movement in cells treated with nocodazole. Large swollen TAT-labeled vesicles of the type shown in Figure 7N were observed in many cells but this was not a universal feature.

Colocalization of dextran with the two peptides in lysosomes was also investigated in KG1a cells, and Figure 8A−C and

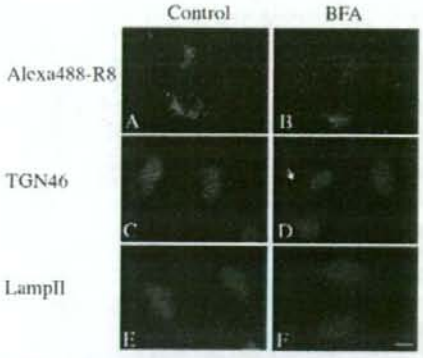

Figure 9. BFA does not affect the subcellular distribution of Alexa488-R8 in HeLa cells. (A−B) HeLa cells were incubated for 120 min with 1 μM Alexa488-R8 prior to incubation for 60 min in control diluent or 5 μg/mL BFA. The cells were then washed visualized by fluorescence microscopy. (C−F) HeLa cells were incubated for 60 min with control diluent or 5 μg/mL BFA prior to fixing and immunostaining with antibodies against TGN46 (C−D) or Lamp-II (E−F) and secondary Alexa594 conjugated anti-sheep (C−D) or anti mouse (E−F) antibodies. The cells were then analyzed by fluorescence microscopy. Arrow denotes BFA induced TGN46 positive tubule. Scale bar 10 μm.

Movie 6 (Supporting Information) show that Alexa488-R8 and dextran both labeled the same more diffusely labeled vesicles. Alexa488-TAT similarly colocalized with dextran in KG1a cells (data not shown). Together, these results demonstrate that TAT and R8 are delivered to lysosomal structures, and this process requires functional actin and microtubular networks.

To confirm that the dextran/peptide-positive organelles were conventional late endosomes and lysosomes, we fixed and labeled KG1a cells containing previously internalized and chased Lysine fixable TxR-dextran with antibodies against the early endosomal marker EEA1 and the late endosome/lysosome marker Lamp-II (*28, 50*). Figure 8D-I shows extensive colocalization between TxR-dextran and Lamp-II but minimal colocalization between EEA1 and dextran. Thus, a 5-h chase period is sufficient to deplete early endocytic organelles of internalized dextran and deliver the ligand to late endocytic, Lamp-II-positive, structures. Similar observations were observed in K562 cells (data not shown).

In view of the fact that we predominantly observed lysosome labeling as opposed to Golgi labeling in leukemia cells, we performed similar experiments in epithelial cells. For this, HeLa lysosomes were similarly labeled with TxR-dextran prior to incubation for 60 min with 3 μM Alexa488-TAT. A representative cell is shown in Figure 8J−L, and this together with Movie 7 (Supporting Information) demonstrates that both labels are located in mobile vesicular structures and short tubules. In agreement with the data from the K562 and KG1a cells, there are numerous examples of vesicles containing both labels, thus demonstrating that a significant fraction of TAT can be delivered to lysosomes within 1 h of incubation. As expected, there were also examples of vesicular structures positive for only one label.

To determine whether peptide distribution in HeLa cells is sensitive to Golgi disruption, cells were incubated with Alexa488-TAT for 120 min prior to a further 60 min incubation in the presence of 5 μg/mL BFA; separate control and BFA treated cells were also fixed and labeled with antibodies against TGN46. In agreement with the data in leukemia cells, BFA had no major effect on the distribution of Alexa488-R8 or -TAT (Figure 9A,B and data not shown). In the presence of BFA, the peptides remained localized in a typical vesicular pattern, enriched to differing extents in the perinuclear region. TGN46 labeling in these cells was highly sensitive to BFA treatment, and the protein dissipated from the perinuclear location to diffuse reticular and tubular structures (Figure 9C,D). We did not find similar TAT peptide-labeled structures in cells treated with BFA. Finally, HeLa cells were incubated with BFA for 60 min and then fixed and labeled with antibodies against Lamp-II and in agreement with our earlier findings, and concordant with other studies (*45*), we observed that the distribution of late endosomes and lysosomes was also predominantly unaffected by BFA treatment (Figure 9E,F).

DISCUSSION

The mechanism of entry and subsequent cellular location of cationic peptides such as those derived from HIV-TAT has received much focus due to their considerable potential as delivery vectors for a range of therapeutic entities. Based on a number of recent observations, there is now widespread acceptance that a large fraction of the material that crosses the plasma membrane does so by an endocytic mechanism. Whether uptake is mediated via a specific plasma membrane domain or receptors is unresolved, as agents that disrupt lipid rafts, macropinocytosis, and clathrin-mediated endocytic events can all inhibit peptide uptake to various extents.

Numerous reports also show that trypsinization and heparin washing can remove a significant fraction of cell-associated peptide confined to the plasma membrane. We and others have however shown that differences in cell-associated fluorescence between peptide incubations performed at 4 °C and 37 °C may be less than 50% (*27, 51*). The latter study also suggested that this is highly dependent on the sequence of the peptide, and that generally the extent of peptide binding at 4 °C is more heterogeneous compared with cells incubated with peptides at 37 °C. In agreement with other studies in HeLa cells (*52*), we observe in both K562 and KG1a cells some heterogeneity in the fluorescent intensities at 37 °C; however, the majority of peptide was confined to vesicular structures. There was very little cell-associated peptide in K562 cells incubated at 4 °C, but this was not the case for KG1a cells, suggesting that they have a very different repertoire of lipids and proteins at the plasma membrane; this may be a reflection of their more primitive differentiation status. Peptide distribution in KG1a cells was highly temperature specific, suggesting that distinct cellular interaction mechanisms operate at low and physiological temperatures.

Though 10 μM amiloride was shown to inhibit approximately 60% of TAT peptide in Namalwa cells (*39*), we previously showed in HeLa cells that 70% R8 uptake occurs in an amiloride insensitive manner (*27*). Here we show that TAT and R8 uptake in K562 cells was relatively insensitive to this drug; together these suggest that macropinocytosis is not the sole entry mechanism for these peptides. K562 cells do not express caveolin 1 and are phenotypically devoid of plasma membrane caveolae (*53*), and therefore, together with the data in HeLa cells, this supports previous observations that caveolae are not required for uptake of TAT and R8 (*16, 54*).

TAT-derived peptides have been localized to vesicular structures containing internalized transferrin, and these could either be early and/or recycling endosomes (*10, 52*). Thus, delivery from the plasma membrane is conventional inasmuch as an early endosome is the first peptide acceptor compartment. The downstream fate of the peptides from these early organelles was, previous to this study, unknown, but increased Antennapedia accumulation in cells treated with the endosomal acidification inhibitor bafilomycin A1 suggested this drug was protecting the peptide from degradation in late endosomes and lysosomes; however, little colocalization of peptides in late endosomes and lysosomes was observed (*14*). TAT uptake was later shown to be dependent on clathrin-coated vesicles and was then transported to an unspecified acidic component (*54*). Since

differential pH quenching experiments with fluorescein and Alexa488 were utilized in this study, it is possible that the peptide-positive organelles could be early or late endosome-like compartments, lysosomes, or possibly even the TGN, a compartment known to have an acidic pH of 6−6.2 (*55*). It was suggested, based on colocalization of BODIPY-ceramide with internalized TAT in HeLa cells and a corresponding lack of colocalization in Lysotracker-positive acidic compartments, that the peptide bypasses late endosomes and lysosomes and traffics to the Golgi. K562 cells have also been utilized for characterizing the uptake of cationic peptides that were shown to be internalized via endocytosis and localized to a perinuclear region, postulated to be of endosomal origin (*56*). Here we show comparable R8 and TAT distribution in K562 cells but extend the observations to show in this cell line and two others that these organelles are most likely lysosomes.

We were initially able to study peptide traffic by virtue of an ability to analyze their subcellular localization in leukemia cells using live cell confocal microscopy and dual labeling. These experiments were aided by the fact that we observed very little plasma membrane labeling at 37 °C, as they were removed from the original peptide-incubation container prior to microscopic analysis. This negated the usual problems of imaging peptide-loaded adherent cells by fluorescence microscopy and allowed for high-resolution spatial analysis of the peptides in organelles.

Internalization of endocytic probes for various time points allowed us to profile distinct subpopulations of endosomes, initially, in the two leukemia cell lines. This revealed major differences in the localization of late endosomes, lysosomes, and peptide-loaded vesicles. There was, however, similar extensive colocalization of dextran with the fluorescent peptides in these cells, after the former was initially allowed to traffic through the endocytic compartment for a minimum of 6 h and a maximum of 8 h. These dextran-labeled organelles should be regarded predominantly as lysosomes, as a number of studies have shown that late endosomes and lysosomes are accessible to plasma membrane-derived molecules within 10−30 min, and typically the half-life for delivery of a fluid phase label or one that is receptor internalized is between 90 and 120 min (*46, 47*). We confirmed this by showing that in fixed cells the dextran-positive compartments are labeled with antibodies against late endosomes and lysosomes but distinct from early endosomes. Previous studies have shown that the perinuclear region in a number of cell lines including K562 is enriched in recycling endosomes (*57*). Although we find transferrin in this region after ~6 min internalization (Figure 7H and data not shown), it does not colocalize to any major extent with TAT that has previously been chased from early endosomes to late endosomes and lysosomes. In agreement with previous observations suggesting a role for microtubules in endosome to lysosome delivery in a number of cell lines, including K562 cells, (*58*), delivery of TAT to dextran-positive lysosomes was inhibited by nocodazole. The drug also caused a redistribution and scattering of lysosomes from the compact perinuclear region, and this is similar to SynB3 peptide labeling in nocodazole-treated K562 cells (*56*). The ability of this drug to inhibit the uptake of cationic peptides in K562 cells was highly sequence specific (*56*), and we observed only a 30% inhibition in nocodazole-treated cells. Cytochalasin D treatment also inhibited the delivery of peptides to lysosomes, suggesting that both an intact actin and microtubule network is required for delivery of these peptides to late endocytic structures.

To refute the possibility that lysosomal labeling of TAT was unique in these leukemia cells, dextran chase experiments were repeated in epithelia cells, and again we found a significant albeit reduced colocalization of the peptides with the lysosomal probe. This reduction in colocalization may reflect obvious differences in endosome dynamics between the cell lines and the possibility in HeLa cells that a greater fraction of the peptide is yet to reach the lysosomes or is trafficked to an alternative compartment(s). Both peptide and dextran were localized together or separately in distinct vesicles rather than in any larger or reticular organelles such as the Golgi and endoplasmic reticulum, respectively. In agreement with our findings that peptides are prevalent only in vesicles, there was a concordant insensitivity of peptide localization to the effects of BFA and a lack of overlap between peptide distribution and Golgi resident proteins. This was clearly shown by us in this study in the leukemia models, most notably in KG1a cells, and in our previous studies in HeLa cells (*28*). It therefore seems unlikely that the Golgi is a major acceptor compartment for these peptides. Fluorescence microscopy utilized in this way does not differentiate between intact and degraded conjugates in any subcellular organelle or the cytosol. As a large fraction of these peptides are delivered to lysosomes, the possibility exists for these and other studies that a heterogeneous population of peptide fragments and possibly free fluorophore are analyzed. Previous studies have shown that R8 and TAT are susceptible to degradation (*14, 59*); however, we previously established that R8 colocalizes extensively with its less proteinase-sensitive D form (*27*). Analysis of peptide stability in these cells lines is now a focus of our research.

Despite our finding of peptide traffic to lysosomes in the three cell lines, it may be as previously mentioned (*54*) that only a very small fraction is required to escape from the endocytic pathway or conceivably enter via a nonendocytic mechanism to elicit a cellular response. The intracellular traffic of these peptides in immature blood cells and epithelia cells as demonstrated in our study mirrors that of the full length HIV TAT protein in T-cells. In Jurkat T-cells the full length TAT protein was shown to be delivered to late endosomes and possibly lysosomes, and of particular significance was that translocation of this protein from the endocytic pathway was dependent on delivery to these late endocytic structures (*20*). Of note in the context of our data with BFA was their observation of very little colocalization of internalized full length TAT with Golgi proteins. On the basis of our observations, we favor a model where peptide translocation to the cytosol also occurs from an endocytic organelle; whether this occurs from an early endosome or a downstream compartment still remains to be determined.

ACKNOWLEDGMENT

The authors would like to thank Birgit Schramm, Brigitte Joggerst-Thomalla (EMBL), and Maria Manunta (Cardiff University) for technical assistance, and Randy Mrsny, Cardiff University, for critical reading of the manuscript. We also thank PerkinElmer and Leica Microsystems for continuous support of the EMBL Advanced Light Microscopy Facility.

Supporting Information Available: Legends for supplemental movies: Movie1. Colocalization (yellow) of TxR-dextran (red) with Alexa488-TAT (green) in lysosomes of K562 cells. Movie 2. Colocalization (yellow) of TxR-dextran (red) with Alexa488-R8 (green) in lysosomes of K562 cells. Movie 3. Localization of TxR-Tf (red) in early/recycling endosomes and Alexa488-R8 (green) in lysosomes of K562 cells. Movie 4. Localization of Alexa488-TAT (green) and lysosomal TxR-dextran (red) in cytochalasin D-treated cells. Movie 5. Localization of Alexa488-TAT (green) and lysosomal TxR-dextran (red) in nocodazole-treated cells. Movie 6. Colocalization (yellow) of TxR-dextran (red) with Alexa488-R8 (green) in lysosomes of KG1a cells. Movie 7. Colocalization (yellow) of TxR-dextran (red) and Alexa488-TAT (green) in lysosomes of HeLa cells. This

material is available free of charge via the Internet at http://pubs.acs.org.

LITERATURE CITED

(1) Joliot, A., and Prochiantz, A. (2004) Transduction peptides: from technology to physiology. *Nat. Cell Biol. 6*, 189−96.

(2) Snyder, E. L., and Dowdy, S. F. (2004) Cell penetrating peptides in drug delivery. *Pharm. Res. 21*, 389−93.

(3) Deshayes, S., Morris, M. C., Divita, G., and Heitz, F. (2005) Cell-penetrating peptides: tools for intracellular delivery of therapeutics. *Cell. Mol. Life Sci. 62*, 1839−49.

(4) Fischer, R., Fotin-Mleczek, M., Hufnagel, H., and Brock, R. (2005) Break on through to the Other Side-Biophysics and Cell Biology Shed Light on Cell-Penetrating Peptides. *Chembiochem*, in press.

(5) Beerens, A. M., Al Hadithy, A. F., Rots, M. G., and Haisma, H. J. (2003) Protein transduction domains and their utility in gene therapy. *Curr. Gene Ther. 3*, 486-94.

(6) Wadia, J. S., and Dowdy, S. F. (2003) Modulation of cellular function by TAT mediated transduction of full length proteins. *Curr. Protein Pept. Sci. 4*, 97−104.

(7) Wadia, J. S., and Dowdy, S. F. (2005) Transmembrane delivery of protein and peptide drugs by TAT-mediated transduction in the treatment of cancer. *Adv. Drug Delivery Rev. 57*, 579−96.

(8) Green, I., Christison, R., Voyce, C. J., Bundell, K. R., and Lindsay, M. A. (2003) Protein transduction domains: are they delivering? *Trends Pharmacol. Sci. 24*, 213−5.

(9) Rudolph, C., Schillinger, U., Ortiz, A., Tabatt, K., Plank, C., Muller, R. H., and Rosenecker, J. (2004) Application of novel solid lipid nanoparticle (SLN)-gene vector formulations based on a dimeric HIV-1 TAT-peptide in vitro and in vivo. *Pharm. Res. 21*, 1662−9.

(10) Richard, J. P., Melikov, K., Vives, E., Ramos, C., Verbeure, B., Gait, M. J., Chernomordik, L. V., and Lebleu, B. (2003) Cell-penetrating peptides. A reevaluation of the mechanism of cellular uptake. *J. Biol. Chem. 278*, 585−90.

(11) Vives, E., Richard, J. P., Rispal, C., and Lebleu, B. (2003) TAT peptide internalization: seeking the mechanism of entry. *Curr. Protein Pept. Sci. 4*, 125−32.

(12) Lundberg, M., Wikstrom, S., and Johansson, M. (2003) Cell surface adherence and endocytosis of protein transduction domains. *Mol. Ther. 8*, 143−50.

(13) Ferrari, A., Pellegrini, V., Arcangeli, C., Fittipaldi, A., Giacca, M., and Beltram, F. (2003) Caveolae-mediated internalization of extracellular HIV-1 tat fusion proteins visualized in real time. *Mol. Ther. 8*, 284−94.

(14) Fischer, R., Kohler, K., Fotin-Mleczek, M., and Brock, R. (2004) A stepwise dissection of the intracellular fate of cationic cell-penetrating peptides. *J. Biol. Chem. 279*, 12625−35.

(15) Tkachenko, A. G., Xie, H., Liu, Y., Coleman, D., Ryan, J., Glomm, W. R., Shipton, M. K., Franzen, S., and Feldheim, D. L. (2004) Cellular trajectories of Peptide-modified gold particle complexes: comparison of nuclear localization signals and Peptide transduction domains. *Bioconjugate Chem. 15*, 482−90.

(16) Wadia, J. S., Stan, R. V., and Dowdy, S. F. (2004) Transducible TAT-HA fusogenic peptide enhances escape of TAT-fusion proteins after lipid raft macropinocytosis. *Nat. Med. 10*, 310−5.

(17) Brooks, H., Lebleu, B., and Vives, E. (2005) Tat peptide-mediated cellular delivery: back to basics. *Adv. Drug Delivery Rev. 57*, 559−77.

(18) Fischer, P. M., Krausz, E., and Lane, D. P. (2001) Cellular delivery of impermeable effector molecules in the form of conjugates with peptides capable of mediating membrane translocation. *Bioconjugate Chem. 12*, 825−41.

(19) Fretz, M. M., Koning, G. A., Mastrobattista, E., Jiskoot, W., and Storm, G. (2004) OVCAR-3 cells internalize TAT-peptide modified liposomes by endocytosis. *Biochim. Biophys. Acta 1665*, 48−56.

(20) Vendeville, A., Rayne, F., Bonhoure, A., Bettache, N., Montcourrier, P., and Beaumelle, B. (2004) HIV-1 Tat enters T cells using coated pits before translocating from acidified endosomes and eliciting biological responses. *Mol. Biol. Cell 15*, 2347−60.

(21) Norgaard, J. M., Olesen, L. H., and Hokland, P. (2004) Changing picture of cellular drug resistance in human leukemia. *Crit. Rev. Oncol. Hematol. 50*, 39−49.

(22) Lea, N. C., Buggins, A. G., Orr, S. J., Mufti, G. J., and Thomas, N. S. (2003) High efficiency protein transduction of quiescent and proliferating primary hematopoietic cells. *J. Biochem. Biophys. Methods 55*, 251−8.

(23) Mazel, M., Clair, P., Rousselle, C., Vidal, P., Scherrmann, J. M., Mathieu, D., and Temsamani, J. (2001) Doxorubicin-peptide conjugates overcome multidrug resistance. *Anticancer Drugs 12*, 107−16.

(24) Rink, H. (1987) Solid-phase synthesis of protected peptide fragments using a trialkoxy-diphenyl-methylester resin. *Tetrahedron Lett. 28*, 3787−3790.

(25) Atherton, E., and Sheppard, R. C. (1989) *Solid-Phase Peptide Synthesis: A Practical Approah*, RL Press, Oxford.

(26) Futaki, S., Ishikawa, T., Niwa, M., Kitagawa, K., and Yagami, T. (1997) Embodying a stable alpha-helical protein structure through efficient chemical ligation via thioether formation. *Bioorg. Med. Chem. 5*, 1883−91.

(27) Nakase, I., Niwa, M., Takeuchi, T., Sonomura, K., Kawabata, N., Koike, Y., Takehashi, M., Tanaka, S., Ueda, K., Simpson, J. C., Jones, A. T., Sugiura, Y., and Futaki, S. (2004) Cellular uptake of arginine-rich peptides: roles for macropinocytosis and actin rearrangement. *Mol. Ther. 10*, 1011−22.

(28) Simpson, J. C., Griffiths, G., Wessling-Resnick, M., Fransen, J. A., Bennett, H., and Jones, A. T. (2004) A role for the small GTPase Rab21 in the early endocytic pathway. *J. Cell Sci. 117*, 6297−311.

(29) Kauppi, M., Simonsen, A., Bremnes, B., Vieira, A., Callaghan, J., Stenmark, H., and Olkkonen, V. M. (2002) The small GTPase Rab22 interacts with EEA1 and controls endosomal membrane trafficking. *J. Cell Sci. 115*, 899−911.

(30) Maxfield, F. R., and McGraw, T. E. (2004) Endocytic recycling. *Nat. Rev. Mol. Cell Biol. 5*, 121−32.

(31) Mellman, I. (1996) Membranes and sorting. *Curr. Opin. Cell Biol. 8*, 497−8.

(32) Baravalle, G., Schober, D., Huber, M., Bayer, N., Murphy, R. F., and Fuchs, R. (2005) Transferrin recycling and dextran transport to lysosomes is differentially affected by bafilomycin, nocodazole, and low temperature. *Cell Tissue Res. 320*, 99−113.

(33) Bright, N. A., Gratian, M. J., and Luzio, J. P. (2005) Endocytic delivery to lysosomes mediated by concurrent fusion and kissing events in living cells. *Curr. Biol. 15*, 360−5.

(34) Shpetner, H., Joly, M., Hartley, D., and Corvera, S. (1996) Potential sites of PI-3 kinase function in the endocytic pathway revealed by the PI-3 kinase inhibitor, wortmannin. *J. Cell Biol. 132*, 595−605.

(35) Backer, J. M. (2000) Phosphoinositide 3-kinases and the regulation of vesicular trafficking. *Mol. Cell Biol. Res. Commun. 3*, 193−204.

(36) Murray, J. W., and Wolkoff, A. W. (2003) Roles of the cytoskeleton and motor proteins in endocytic sorting. *Adv. Drug. Delivery Rev. 55*, 1385−403.

(37) West, M. A., Bretscher, M. S., and Watts, C. (1989) Distinct endocytotic pathways in epidermal growth factor-stimulated human carcinoma A431 cells. *J. Cell Biol. 109*, 2731−9.

(38) Rich, I. N., Worthington-White, D., Garden, O. A., and Musk, P. (2000) Apoptosis of leukemic cells accompanies reduction in intracellular pH after targeted inhibition of the Na(+)/H(+) exchanger. *Blood 95*, 1427−34.

(39) Kaplan, I. M., Wadia, J. S., and Dowdy, S. F. (2005) Cationic TAT peptide transduction domain enters cells by macropinocytosis. *J. Controlled Release 102*, 247−53.

(40) Bright, N. A., Lindsay, M. R., Stewart, A., and Luzio, J. P. (2001) The relationship between lumenal and limiting membranes in swollen late endocytic compartments formed after wortmannin treatment or sucrose accumulation. *Traffic 2*, 631−42.

(41) Fernandez-Borja, M., Wubbolts, R., Calafat, J., Janssen, H., Divecha, N., Dusseljee, S., and Neefjes, J. (1999) Multivesicular body morphogenesis requires phosphatidyl-inositol 3- kinase activity. *Curr. Biol. 9*, 55−8.

(42) Lippincott-Schwartz, J., Yuan, L. C., Bonifacino, J. S., and Klausner, R. D. (1989) Rapid redistribution of Golgi proteins into the ER in cells treated with brefeldin A: evidence for membrane cycling from Golgi to ER. *Cell 56*, 801−13.

(43) Doms, R. W., Russ, G., and Yewdell, J. W. (1989) Brefeldin A redistributes resident and itinerant Golgi proteins to the endoplasmic reticulum. *J. Cell Biol. 109*, 61−72.

(44) Lippincott-Schwartz, J., Donaldson, J. G., Schweizer, A., Berger, E. G., Hauri, H. P., Yuan, L. C., and Klausner, R. D. (1990) Microtubule-dependent retrograde transport of proteins into the ER

in the presence of brefeldin A suggests an ER recycling pathway. *Cell 60*, 821−36.
(45) Reaves, B., and Banting, G. (1992) Perturbation of the morphology of the trans-Golgi network following Brefeldin A treatment: redistribution of a TGN-specific integral membrane protein, TGN38. *J. Cell Biol. 116*, 85−94.
(46) Green, S. A., Zimmer, K. P., Griffiths, G., and Mellman, I. (1987) Kinetics of intracellular transport and sorting of lysosomal membrane and plasma membrane proteins. *J. Cell Biol. 105*, 1227−40.
(47) Griffiths, G., Back, R., and Marsh, M. (1989) A quantitative analysis of the endocytic pathway in baby hamster kidney cells. *J. Cell Biol. 109*, 2703−20.
(48) Collot, M., Louvard, D., and Singer, S. J. (1984) Lysosomes are associated with microtubules and not with intermediate filaments in cultured fibroblasts. *Proc. Natl. Acad. Sci. U.S.A. 81*, 788−92.
(49) Gruenberg, J., Griffiths, G., and Howell, K. E. (1989) Characterization of the early endosome and putative endocytic carrier vesicles in vivo and with an assay of vesicle fusion in vitro. *J. Cell Biol. 108*, 1301−16.
(50) Kuronita, T., Eskelinen, E. L., Fujita, H., Saftig, P., Himeno, M., and Tanaka, Y. (2002) A role for the lysosomal membrane protein LGP85 in the biogenesis and maintenance of endosomal and lysosomal morphology. *J. Cell Sci. 115*, 4117−31.
(51) Saalik, P., Elmquist, A., Hansen, M., Padari, K., Saar, K., Viht, K., Langel, U., and Pooga, M. (2004) Protein cargo delivery properties of cell-penetrating peptides. A comparative study. *Bioconjugate Chem. 15*, 1246−53.
(52) Potocky, T. B., Menon, A. K., and Gellman, S. H. (2003) Cytoplasmic and nuclear delivery of a TAT-derived peptide and a beta-peptide after endocytic uptake into HeLa cells. *J. Biol. Chem. 278*, 50188−94.
(53) Scherer, P. E., Lewis, R. Y., Volonte, D., Engelman, J. A., Galbiati, F., Couet, J., Kohtz, D. S., van Donselaar, E., Peters, P., and Lisanti, M. P. (1997) Cell-type and tissue-specific expression of caveolin-2. Caveolins 1 and 2 co-localize and form a stable heterooligomeric complex in vivo. *J. Biol. Chem. 272*, 29337−46.
(54) Richard, J. P., Melikov, K., Brooks, H., Prevot, P., Lebleu, B., and Chernomordik, L. V. (2005) Cellular uptake of unconjugated TAT peptide involves clathrin-dependent endocytosis and heparan sulfate receptors. *J. Biol. Chem. 280*, 15300−15306.
(55) Weisz, O. A. (2003) Organelle acidification and disease. *Traffic 4*, 57−64.
(56) Drin, G., Cottin, S., Blanc, E., Rees, A. R., and Temsamani, J. (2003) Studies on the internalization mechanism of cationic cell-penetrating peptides. *J. Biol. Chem. 278*, 31192−201.
(57) Green, E. G., Ramm, E., Riley, N. M., Spiro, D. J., Goldenring, J. R., and Wessling-Resnick, M. (1997) Rab11 is associated with transferrin-containing recycling compartments in K562 cells. *Biochem. Biophys. Res. Commun. 239*, 612−6.
(58) Jin, M., and Snider, M. D. (1993) Role of microtubules in transferrin receptor transport from the cell surface to endosomes and the Golgi complex. *J. Biol. Chem. 268*, 18390−7.
(59) Gammon, S. T., Villalobos, V. M., Prior, J. L., Sharma, V., and Piwnica-Worms, D. (2003) Quantitative analysis of permeation peptide complexes labeled with Technetium-99m: chiral and sequence-specific effects on net cell uptake. *Bioconjugate Chem. 14*, 368−76.

BC050274H

THE JOURNAL OF BIOLOGICAL CHEMISTRY VOL. 281, NO. 6, pp. 3544–3551, February 10, 2006

High Density of Octaarginine Stimulates Macropinocytosis Leading to Efficient Intracellular Trafficking for Gene Expression*[S]

Received for publication, March 23, 2005, and in revised form, October 27, 2005 Published, JBC Papers in Press, December 2, 2005, DOI 10.1074/jbc.M503202200

Ikramy A. Khalil[‡§], Kentaro Kogure[‡§], Shiroh Futaki[¶‖], and Hideyoshi Harashima[‡§1]

From the [‡]Graduate School of Pharmaceutical Sciences, Hokkaido University, Kita-12, Nishi-6, Kita-ku, Sapporo, Hokkaido 060-0812, the [§]Core Research for Evolutional Science and Technology and [¶]Precursory Research for Embryonic Science and Technology, Japan Science and Technology Agency, 3-1-6 Shibuya, Shibuya-ku, Tokyo 150-0002, and the [‖]Institute for Chemical Research, Kyoto University, Uji, Kyoto 611-0011, Japan

The mechanism of the arginine-rich peptide-mediated cellular uptake is currently a controversial issue. Several factors, including the type of peptide, the nature of the cargo, and the linker between them, appear to affect uptake. One of the less studied factors, which may affect the uptake mechanism, is the effect of peptide density on the surface of the cargo. Here, we examined the mechanism of cellular uptake and intracellular trafficking of liposomes modified with different densities of the octaarginine (R8) peptide. Liposomes modified with a low R8 density were taken up mainly through clathrin-mediated endocytosis, leading to extensive lysosomal degradation, whereas those modified with a high R8 density were taken up mainly through macropinocytosis and were less subject to lysosomal degradation. Furthermore, the high density R8-liposomes were able to stimulate the macropinocytosis-mediated uptake of other particles. When plasmid DNA was condensed and encapsulated in R8-liposomes, the levels of gene expression were three orders of magnitude higher for the high density liposomes. The enhanced gene expression by the high density R8-liposomes was highly impaired by blocking uptake through macropinocytosis. The different extents of gene expression from different densities of the R8 peptide on the liposomes could be explained principally by the existence of an intracellular trafficking route, but not by the uptake amount, of internalized liposomes. These results show that the density of the R8 peptide on liposomes determines the uptake mechanism and that this is directly linked to intracellular trafficking, resulting in different levels of gene expression.

The human immunodeficiency virus TAT[2]-derived peptide is a small basic peptide that has been shown to successfully mediate the efficient cellular uptake of a wide variety of cargos, including proteins, peptides, and nucleic acids (1–3). Torchilin *et al.* (4) recently demonstrated that even certain TAT-linked liposomes with a diameter of 200 nm could be efficiently internalized into a variety of cell lines in intact form. The attachment of TAT directly to the liposome surface without a spacer or the presence of high molecular weight polyethylene glycol spacers abolished liposome internalization, indicating the importance of the direct contact of TAT with the cell surface (4). More recently, other groups reported an enhanced cellular uptake of liposomes when modified with TAT peptide (5, 6). Complexes formed between TAT-liposomes and DNA also showed enhanced transfection *in vitro* and *in vivo* (7).

Despite the well demonstrated ability of TAT to internalize different cargos, the internalization mechanism of the peptide itself or its cargo remains a controversial issue. According to early studies, none of the classic receptor-, transporter-, or endocytosis-mediated processes seemed to be involved in the uptake of TAT and other similar peptides (8, 9). Direct penetration- and inverted micelle-driven delivery have been suggested as possible internalization mechanisms (10). However, the mechanism of entry was recently re-evaluated based on possible problems that may occur due to cell fixation prior to microscopy observation, and more evidence appeared to support the involvement of endocytosis (11, 12). Endocytosis-mediated uptake is also a controversial issue, because various findings showing the involvement of different endocytic mechanisms have been reported (11–18).

The TAT sequence, which is critical for translocation, contains several arginine residues (19). Homopolymers of arginine are similar to the TAT peptide in terms of efficiency and uptake mechanism (19, 20), making them a possible candidate for mimicking the TAT peptide. The optimum number of arginine residues for efficient internalization was shown to be ~8 residues (19). The octaarginine (R8) peptide could mediate the efficient intracellular delivery of macromolecules, and similar to the TAT peptide but less studied, the exact uptake mechanism of R8-cargos is still largely unknown.

The diversity of results regarding the uptake mechanism of arginine-rich peptides suggests that some factors may affect the entry mechanism. These factors include the type of peptide, its mode of exposure to the cell surface, the nature of the cargo, and the chemical linkage between the peptide and the cargo (21). For example, we have previously shown that the R8 peptide and its complexes with DNA were taken up by different mechanisms, suggesting that the nature of the interaction between the peptide and the cell surface (*i.e.* the peptide in free or complexed state) affects the uptake mechanism (22). Another possible factor that has been less studied is the effect of peptide density on the

* This work was supported by Grants-in-Aid for Scientific Research (B) from the Ministry of Education, Culture, Sports, Science and Technology of Japan, and by Grants-in-Aid for Scientific Research on Priority Areas from the Japan Society for the Promotion of Science. The costs of publication of this article were defrayed in part by the payment of page charges. This article must therefore be hereby marked "*advertisement*" in accordance with 18 U.S.C. Section 1734 solely to indicate this fact.

[S] The on-line version of this article (available at http://www.jbc.org) contains supplemental Figs. S1–S3.

[1] To whom correspondence should be addressed. Tel.: 81-11-706-3919; Fax: 81-11-706-4879; E-mail: harasima@pharm.hokudai.ac.jp.

[2] The abbreviations used are: TAT, transactivator of transcription; R8, octaarginine peptide; EPC, egg phosphatidylcholine; Chol, cholesterol; Rh-PE, *N*-(lissaminerhodamine-B-sulfonyl)-1,2-dipalmitoyl-*sn*-glycero-3-phosphoethanolamine; NBD, 1,2-dipalmitoyl-*sn*-glycero-3-phosphoethanolamine-*N*-(7-nitro-2-1,3-benzoxadiazol-4-yl); DOPE,dioleoylphosphatidylethanolamine; CHEMS, cholesteryl hemisuccinate; STR-R8, stearylated-octaarginine; R8-Lip, octaarginine-modified liposomes; R8-Lip-HD, R8-Lip modified with a high density of STR-R8 (5.2 mol % of total lipid); R8-Lip-LD, R8-Lip modified with a low peptide density (0.86 mol % of total lipid); R8-Cps, R8-modified DNA-coated particles; HSPG, heparan sulfate proteoglycan; PTD, protein transduction domain; Tf, transferrin, ND, neutral dextran; R8-Lip-LD-RA, R8-Lip-LD containing rhodamine aqueous phase; R8-Lip-HD-E, empty R8-Lip-HD; MF, mean fluorescence; RLU, relative light units; TMR, tetramethylrhodamine; FITC, fluorescein isothiocyanate; PBS, phosphate-buffered saline.

internalization mechanism. It was previously shown that a single TAT peptide was sufficient to allow the cellular delivery of an unfolded fusion construct of the same protein (23). Other studies showed that several TAT peptides attached to the surface of the cargo were required to permit efficient cellular delivery (24). However, no direct comparison to show the effect of peptide density on the uptake mechanism was conducted. Liposomes are good tools for use in such a comparison, because their surface can be easily modified with different densities of peptide and they can provide localized areas of high peptide density that are available to interact with the cell membrane. Therefore, the main purpose of this study was to investigate the effect of peptide density on the internalization mechanism and intracellular trafficking of cargos modified with arginine-rich peptides. The R8 peptide was chosen as a prototype of arginine-rich peptides and liposomes were chosen as an example of cargos.

Here, we present results showing that the mechanism of uptake of liposomes modified with a low R8 density shifted from clathrin-mediated endocytosis to macropinocytosis when the density of R8 was increased. The uptake route influenced intracellular trafficking, resulting in a remarkable difference in gene expression when condensed plasmid DNA was encapsulated into each type of liposome. These results highlight important features concerning the mechanism of entry and intracellular fate of R8-modified nanoparticles and demonstrate the role of the peptide density in determining the cellular uptake pathways of cargos. Furthermore, the data provided here indicate that uptake through macropinocytosis is more efficient in terms of avoiding lysosomal degradation resulting in an enhanced gene expression.

EXPERIMENTAL PROCEDURES

Materials—Egg phosphatidylcholine (EPC), cholesterol (Chol), *N*-(lissaminerhodamine-B-sulfonyl)-1,2-dipalmitoyl-*sn*-glycero-3-phosphoethanolamine (Rh-PE), 1,2-dipalmitoyl-*sn*-glycero-3-phosphoethanolamine-*N*-(7-nitro-2-1,3-benzoxadiazol-4-yl) (NBD-PE), and dioleoylphosphatidylethanolamine (DOPE) were purchased from Avanti Polar Lipids (Alabaster, AL). Sulforhodamine B, Syto-24, tetramethylrhodamine-labeled neutral dextran (70 kDa), FITC-labeled transferrin, and LysoSensor Green were purchased from Molecular Probes (Eugene, OR). Cholesteryl hemisuccinate (CHEMS), poly-L-lysine, amiloride, and filipin were purchased from Sigma-Aldrich. Stearylated-octaarginine was synthesized as described previously (25). Other chemicals were purchased from Wako Chemicals (Osaka, Japan). Plasmid DNA Pcmv-luc-encoding luciferase was prepared by using an EndFree Plasmid Mega Kit (Qiagen, Hilden, Germany). NIH3T3 cells were obtained from the American Type Culture Collection (Manassas, VA).

Preparation of the Octaarginine-modified Liposomes—Liposomes were basically composed of EPC and Chol (7:3 molar ratio), and stearylated-R8 (STR-R8) was incorporated at 0–10 mol % of the total lipid. To label the lipid phase, Rh-PE or NBD-phosphoethanolamine was incorporated at 1 mol % of the total lipid. Liposomes were prepared by hydration method followed by extrusion with a Mini-Extruder (Avanti Polar Lipids), through polycarbonate membrane filters (Nucleopore) of 400, 200, and 100 nm. Sulforhodamine B was used as an aqueous phase marker, when required. Liposomes were purified on a Bio-Gel A-1.5m column (100–200 mesh). The particle sizes of the liposomes were measured by a quasi-elastic light scattering method, and the zeta potential was determined by means of an electrophoretic light scattering spectrophotometer (ELS-8000, Photal Otsuka Electronics).

Preparation of the Octaarginine-modified DNA-coated Particles—Plasmid DNA was condensed with poly-L-lysine as described previously (26). A condensed DNA solution was then added to the lipid film, formed by the evaporation of a chloroform solution of the lipids: EPC/Chol/STR-R8 (7:3:0.086 or 0.52 molar ratio), or DOPE/CHEMS (9:2 molar ratio) on the bottom of a glass tube, followed by incubation for 10 min to hydrate the lipid film. The glass tube was then sonicated for ~1 min in a bath-type sonicator (125 W, Branson Ultrasonics, Danbury, CT). In the case of DOPE/CHEMS, the particles, after sonication, were incubated with an aqueous solution of STR-R8 (0.86 or 5.2 mol % of total lipids) for 30 min at room temperature. The size and zeta potential of the coated particles were measured as described above.

Confocal Laser Microscopy—To investigate the cellular uptake of the R8-modified liposomes (R8-Lip), NIH3T3 cells were treated with double-labeled R8-Lip (NBD-labeled lipid and rhodamine-labeled aqueous phase, final concentration of 0.1 mM lipid) in serum-free medium at 37 °C for 1 h. The cells were then washed 3 times with ice-cold PBS and analyzed by confocal laser microscopy (LSM510, Carl Zeiss). To investigate the mechanism of internalization of R8-Lip, cells were incubated in the absence or presence of sucrose (0.4 M) for 30 min or amiloride (5 mM) for 10 min. Different R8-liposomes, containing a rhodamine aqueous phase, were then added, and the incubation was continued for 1 h. The cells were then washed 3 times with ice-cold PBS supplemented with heparin and observed by confocal microscopy. Nuclei were stained with Syto-24 in the last 20 min of incubation. For the colocalization study, in the case of transferrin, cells were first incubated with R8-Lip containing rhodamine aqueous phase for 30 min, the medium was then removed, a new medium containing FITC-labeled transferrin (5 μM) was added, and incubation was continued for 5 min before observation within 5 min. In the case of neutral dextran, NBD-labeled R8-liposomes were added to cells followed by adding tetramethylrhodamine-labeled neutral dextran (5 μM) and incubation continued for 30 min. The medium was then exchanged with liposome-free medium containing neutral dextran followed by incubation for 10 min. Cells were then washed with ice-cold PBS and observed. To investigate the intracellular fate of the liposomes, NIH3T3 cells were treated with different R8-liposomes containing an aqueous rhodamine phase at 37 °C for 30 min. The medium was then removed; the cells were washed with new medium, incubated in fresh liposome-free medium for a total of 1, 3, or 6 h, and then observed with confocal microscopy. Nuclei were stained with Syto-24 in the last 20 min of incubation. The same experiment was repeated using R8-Lip modified with low density of STR-R8 and containing rhodamine aqueous phase in the absence or presence of non-labeled R8-Lip modified with a high density of STR-R8 (a 5-fold increase, calculated as R8 content). To quantify the intracellular fluorescence, the total pixel areas of the fluorescence were measured using AquaCosmos software (Hamamatsu Photonics, Hamamatsu, Japan). To investigate the colocalization of R8-Lip with lysosomes, cells were incubated with different R8-Lip preparations containing rhodamine aqueous phase at 37 °C for 30 min. The medium was then removed; the cells were washed with new medium and incubated in fresh liposome-free medium for a total of 3 h. Thirty minutes before observation by confocal microscopy, the LysoSensor was applied at a final concentration of 1 μM to stain the acidic compartments.

Flow Cytometry—To investigate the cellular uptake of R8-Lip, NIH3T3 cells were incubated in serum-free medium containing different R8-Lip (final concentration, 0.1 mM lipids) for 1 h at 37 °C. At the end of the incubation, the medium was removed, and the cells were washed once with ice-cold PBS with or without heparin (20 units.ml^{-1}). The cells were then trypsinized and washed twice by centrifugation at 4 °C (± heparin), suspended in 1 ml of PBS, and, after passing through a nylon mesh, they were analyzed by flow cytometry (BD Biosciences). To

investigate the cellular association in the presence of heparin, NIH3T3 cells were incubated in serum-free medium containing increasing concentrations of heparin for 5 min at 37 °C. Different R8-Lip preparations containing rhodamine aqueous phase were then added, and the incubation was continued for 1 h. At the end of the incubation, the medium was removed, and the cells were washed once with ice-cold PBS, trypsinized, washed twice by centrifugation at 4 °C, suspended in 1 ml of PBS, passed through a nylon mesh, and analyzed by flow cytometry. To examine the mechanism of internalization of R8-Lip, cells were incubated in the absence or presence of a mixture of metabolic inhibitors (sodium azide, 0.1%, sodium fluoride, 10 mM, and antimycin A, 1 $\mu g.ml^{-1}$) for 30 min, sucrose (0.4 M) for 30 min, amiloride (5 mM) for 10 min, or filipin (1 $\mu g.ml^{-1}$) for 1 h. Different R8-Lip preparations, containing rhodamine aqueous phase, were then added, and the incubation was continued for 1 h. Then cells were analyzed by flow cytometry after washing 3 times with PBS supplemented with heparin, as described above. To investigate the uptake of neutral dextran, cells were incubated with tetramethylrhodamine-labeled neutral dextran (5 μM) in the presence or absence of empty (non-labeled) R8-Lip modified with a high density of STR-R8 for 30 min at 37 °C then analyzed. To investigate the stimulation of macropinocytosis, cells were incubated with R8-Lip modified with low density of STR-R8 and containing a rhodamine aqueous phase mixed with increasing concentrations of empty (non-labeled) R8-Lip modified with a high density of STR-R8 for 1 h at 37 °C. The experiment was performed in the presence or absence of amiloride (5 mM) to inhibit macropinocytic uptake.

Transfection Assay—One day before transfection, NIH3T3 cells were seeded into 24-well plates at 4×10^4 cells per well. Cells were incubated for 1 h at 37 °C with 0.25 ml of serum-free medium containing different R8-modified DNA-coated particles containing 0.4 μg of DNA. Next, 1 ml of medium containing 10% fetal calf serum was added, and the incubation continued for an additional 23 h. The cells were then washed and solubilized with reporter lysis buffer (Promega, Madison, WI). Luciferase activity in the cell lysate was then measured by means of a luminometer (Luminescencer-PSN, ATTO, Japan). The amount of protein in the cell lysate was determined using a BCA protein assay kit (Pierce). To investigate the contribution of different uptake pathways in gene expression, cells were pretreated with or without sucrose (0.4 M) or amiloride (2.5 mM) for 10 min and R8-modified DNA-coated particles (lipid composition DOPE/CHEMS) containing 5.2 mol % STR-R8 were then added, and the incubation was continued for 1 h. The medium was then removed, and the cells were washed 3 times with PBS containing 20 $units.ml^{-1}$ heparin and once with PBS. The cells were then incubated in the presence of serum-free medium for 70 min followed by further incubation in the presence of 1 ml of medium containing 10% FBS for periods of up to 12 h. To control the effects of sucrose or amiloride on intracellular events, cells were first loaded with R8-modified DNA-coated particles for 1 h, then washed and incubated for 70 min in the presence of these reagents, after which, 1 ml of medium containing 10% fetal bovine serum was added, and the cells were further incubated for a total of 12 h.

RESULTS

Preparation and Characterization of Octaarginine-modified Liposomes—A series of R8-Lip containing various concentrations of STR-R8 peptide was prepared. In this preparation, the stearyl moiety acts as an anchor to the lipid membrane leaving the R8 peptide freely attached to the surface. The zeta potential of the prepared liposomes was determined as a measure of their net charge (Fig. 1*A*). Increasing the concentration of STR-R8 peptide caused an initial rapid increase in zeta potential followed by a slower increase for concentrations up to ~5 mol %. No further increase in zeta potential was observed >5 mol % STR-R8, indicating that the liposomal surface was saturated with the cationic peptide. In the next experiments, we chose liposomes modified with a low density (0.86 mol %) of STR-R8 (R8-Lip-LD), which had a low positive charge, and those modified with a high density (5.2 mol %) of STR-R8 (R8-Lip-HD), which had the highest possible positive charge. Data related to the characterization of the different liposomes used in this study are shown in Table 1.

Cellular Uptake of R8-liposomes—First, we quantitatively compared the cellular uptake of R8-Lip-LD and R8-Lip-HD containing an aqueous rhodamine phase by flow cytometry. We confirmed that the surface-bound liposomes could be removed by means of heparin wash (data not shown). The measured intracellular fluorescence in the case of R8-Lip-HD was higher than that for R8-Lip-LD by less than one order of magnitude (Fig. 1*B*). When we measured the total fluorescence (surface-bound plus internalized liposomes) by excluding the heparin washes, we found that the fluorescence in the case of R8-Lip-HD was about one order of magnitude higher than that in the case of R8-Lip-LD (data not shown). Liposomes that were devoid of STR-R8 did not show any intracellular or surface-bound fluorescence (data not shown). The cellular uptake of both liposomes was further confirmed using confocal laser microscopy of living cells (supplemental Fig. S1). Surface-bound fluorescence was higher in the case of R8-Lip-HD. Taken together; these results indicate that both R8-Lip-LD and R8-Lip-HD can bind to the cell surface, especially R8-Lip-HD, and that they are efficiently internalized.

Transfection Activities of R8-Lip Containing Plasmid DNA—Because R8-Lip showed a high potential for the intracellular delivery of macromolecules encapsulated in their cores, we investigated the cellular uptake of R8-Lip-containing plasmid DNA, for use in gene delivery. We prepared condensed DNA particles coated with a lipid envelope consisting of EPC and Chol and modified with the R8 peptide (R8-modified coated particles, R8-Cps) as described under "Experimental Procedures." We incubated the cells for 1 h with R8-Cps containing FITC-labeled DNA modified with 0.86 or 5.2 mol % STR-R8 (R8-Cps-LD and R8-Cps-HD) and then observed the cells by confocal microscopy. In both cases, the intracellular fluorescence was similar to the pattern of distribution obtained earlier with R8-Lip (data not shown), indicating the efficient cellular uptake of plasmid DNA encapsulated in the R8-Lip. We next investigated the transfection efficiency of R8-Cps containing plasmid DNA encoding a luciferase reporter gene. R8-Cps-LD did not show a significant gene expression, whereas the R8-Cps-HD produced gene expression levels about 3 orders of magnitude higher (Fig. 1*C*). This difference in gene expression is not correlated with the difference in cellular uptake as indicated by flow cytometry and confocal microscopy. Therefore, the superiority of the R8-Cps-HD regarding gene expression cannot be explained by differences in the amount of DNA internalized, but that there are intracellular events responsible for this difference.

Mechanism of Uptake of Different R8-liposomes—Because the gene expression levels of the R8-Cps were not correlated with the amount of liposomes internalized, we investigated the mechanism of uptake of different R8-Lip as a candidate to explain the difference in the intracellular fate of the particles. It has previously been shown that the cell-surface heparan sulfate proteoglycans (HSPGs) act as nonspecific receptors in the cellular binding of different protein transduction domain (PTD) peptides (27, 28). As mentioned above, several washings with a buffer containing heparin were sufficient to remove the surface-bound liposomes. Furthermore, the addition of heparin to the medium prior to the addition of R8-Lip dramatically inhibited the cellular bind-

ing and internalization of R8-Lip especially in the case of R8-Lip-LD (supplemental Fig. S1). In both cases, concentrations as low as 1 unit·ml^{-1} were sufficient to completely block the interaction of the liposomes with the cell surface. Taken together, these data probably show the involvement of cell-surface HSPGs in the uptake of R8-Lip, similar to other PTD-liposomes (6).

To investigate the contribution of the endocytic pathway in the internalization of R8-Lip, we incubated cells with R8-Lip-LD or R8-Lip-HD in the presence or absence of a mixture of metabolic inhibitors that inhibit all types of endocytosis through energy depletion (29) and then measured the internalized liposomes using flow cytometry. As shown in Fig. 2, the metabolic inhibitors strongly inhibited the uptake of both types of liposomes, indicating that the uptake process is highly energy-dependent and supporting the contribution of endocytosis as a major uptake pathway in the case of R8-Lip. We next investigated the contribution of different endocytic uptake pathways that have been characterized to date, using specific inhibitors of each type (30–34). Clathrin-mediated endocytosis is the major and best characterized endocytic pathway (30). Macropinocytosis and caveolae represent other types of clathrin-independent endocytosis (31–34). We examined the effects of the following inhibitors: a hypertonic medium to specifically inhibit clathrin-mediated endocytosis through dissociation of the clathrin lattice (30), amiloride to specifically inhibit macropinocytosis by inhibiting the Na^+/H^+ exchange required for macropinocytosis (14, 30), and filipin to specifically inhibit caveolar uptake through cholesterol depletion (17, 30). The use of a hypertonic medium strongly inhibited the uptake of R8-Lip-LD, whereas it inhibited the uptake of R8-Lip-HD by ~35%. This indicated that clathrin-mediated endocytosis is the major uptake pathway of R8-Lip-LD, whereas the uptake of R8-Lip-HD probably involves different pathways as a major entrance route. Surprisingly, in the presence of the macropinocytosis inhibitor amiloride, >50% of the particles were internalized in the case of R8-Lip-LD, whereas only 20% were internalized in the case of R8-Lip-HD. Taken together, these results indicate that only the R8-Lip modified with high amounts of R8 peptide uses macropinocytosis as the major entrance route, whereas those modified with a low density of R8 mainly use the classic clathrin-mediated endocytosis. The caveolar inhibitor filipin inhibited the uptake of both liposomes only slightly, indicating the minor contribution of caveolae in the uptake process. The effects of sucrose and amiloride were confirmed by confocal microscopy observations of living cells (supplemental Fig. S2). Cytochalasin D and nystatin, both of which can inhibit macropinocytosis and caveolae (30), inhibited the uptake of R8-Lip-HD (data not shown). Because the presence of the specific caveolae inhibitor, filipin, caused only a minor inhibition of uptake, these results further confirm the involvement of macropinocytosis in the uptake.

Colocalization between R8-Lip and Different Endocytosis Markers—Transferrin (Tf) is a well known marker for the internalization through clathrin-mediated endocytosis (35). Neutral dextran, 70 kDa (ND), is a fluid phase marker that can be used to trace the internalization via macropinocytosis (14). We performed a colocalization study between R8-Lip and these markers using confocal microscopy (Fig. 3). Intracellular R8-Lip-LD was highly colocalized with Tf, whereas R8-Lip-HD did not show any significant colocalization with Tf under the same conditions. In the case of the fluid phase marker ND, most of the intracellular liposomes were colocalized with the marker in large intracellular vesicles in the case of R8-Lip-HD, whereas only a partial colocalization was observed in the case of R8-Lip-LD. The partial colocalization in the case of R8-Lip-LD is consistent with the result shown in Fig. 2, which shows that amiloride partially inhibited uptake. These results show that R8-Lip-HD and Tf mainly use distinctive internalization pathways, whereas there is a high contribution of the clathrin-mediated endocytosis in the case of R8-Lip-LD. Bodipy-LacCer, a marker of caveolae

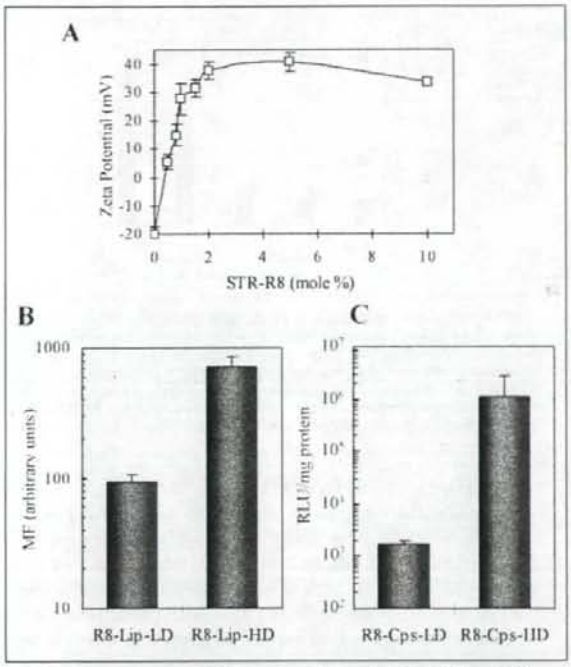

FIGURE 1. **Characterization, cellular uptake, and transfection activities of different octaarginine-modified liposomes or DNA-coated particles.** *A*, zeta potentials for different R8-liposomes (R8-Lip) containing increasing concentrations of stearylated octaarginine (STR-R8). Each point represents the mean ± S.D. of at least two different preparations measured in triplicates. *B*, flow cytometric analysis of cells incubated for 1 h with liposomes modified with low density (R8-Lip-LD) or high density (R8-Lip-HD) of R8 and containing rhodamine aqueous phase. The mean fluorescence (*MF*) of 10,000 cells is shown. *Error bars* represent the ±S.D. for three different experiments performed in duplicate. *C*, transfection activities of DNA-coated particles modified with low density (R8-Cps-LD) or high density (R8-Cps-HD) of the R8 peptide and prepared with a lipid envelope containing EPC/Chol. Luciferase activities were measured as described under "Experimental Procedures" 24 h after transfection and are expressed as the relative light unit (*RLU*) per milligram of protein. Data represent the mean ± S.D. of three different experiments performed in triplicate.

TABLE 1
Characterization of R8-modified liposomes

	Lipid composition (molar ratio)	Diameter[a]	Zeta potential[a]
		nm	*mV*
R8-Lip-LD-RA[b]	EPC:Chol:STR-R8 (7:3:0.086)	152 ± 18	13 ± 11
R8-Lip-HD-RA[b]	EPC:Chol:STR-R8 (7:3:0.52)	102 ± 10	35 ± 4
R8-Lip-LD-FL[c]	EPC:Chol:NBD-PE:STR-R8 (7:3:0.1:0.085)	170 ± 2	7 ± 1
R8-Lip-HD-FL[c]	EPC:Chol:NBD-PE:STR-R8 (7:3:0.1:0.52)	149 ± 3	40 ± 1

[a] Data represent means ± S.D. of at least two different determinations.
[b] RA, liposomes containing rhodamine-labeled aqueous phase.
[c] FL, liposomes containing NBD-labeled lipid phase.

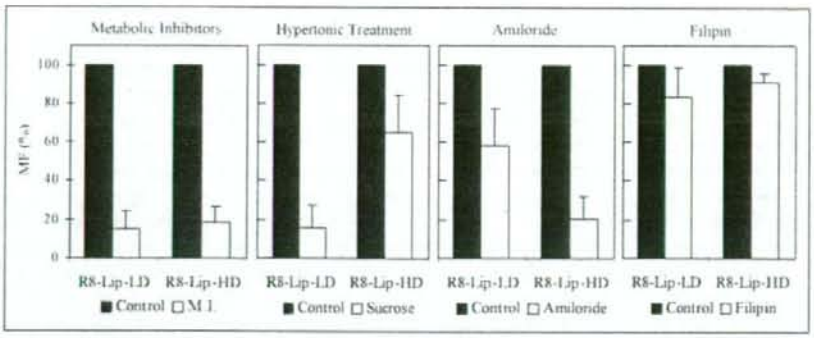

FIGURE 2. **Mechanism of cellular uptake of different R8-liposomes.** NIH3T3 cells were incubated for 1 h with liposomes modified with low or high density of STR-R8 (R8-Lip-LD or R8-Lip-HD) and containing rhodamine aqueous phase in the absence or the presence of a mixture of metabolic inhibitors (*M.I.*) (sodium azide, 0.1%, sodium fluoride, 10 mM, and antimycin A, 1 $\mu g.ml^{-1}$), a hypertonic medium (sucrose, 0.4 M), the macropinocytosis inhibitor amiloride (5 mM), or the caveolar inhibitor filipin (1 $\mu g.ml^{-1}$). The mean fluorescence (*MF*) of 10,000 cells was measured by flow cytometry and is expressed as the percentage of the fluorescence measured in the absence of the inhibitors. *Error bars* represent the ±S.D. for three different experiments performed in duplicate.

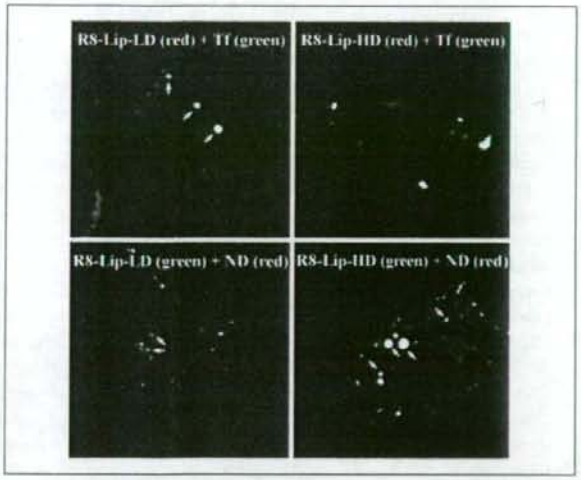

FIGURE 3. **Colocalization between different R8-liposomes and different endocytosis markers.** NIH/3T3 cells were incubated with R8-Lip-LD or R8-Lip-HD containing an aqueous rhodamine phase for 30 min and FITC-labeled transferrin (*Tf*) was then added, and the incubation continued for 5 min before observation by confocal microscopy. In the case of neutral dextran 70 kDa (*ND*), cells were incubated with R8-Lip-LD or R8-Lip-HD containing NBD-lipid phase then ND labeled with tetramethylrhodamine (*TMR*) was added, and incubation continued for 30 min followed by another incubation for 10 min in the presence of liposome-free medium containing ND. *Arrows* indicate intracellular liposomes colocalized with the endocytosis markers.

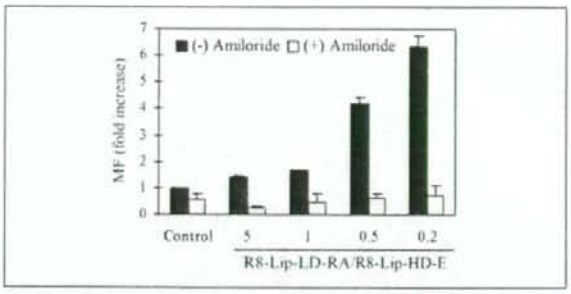

FIGURE 4. **Stimulation of macropinocytosis.** NIH3T3 cells were incubated for 1 h with R8-Lip-LD containing rhodamine aqueous phase (R8-Lip-LD-RA) in the presence of increasing concentrations of empty (non-labeled) R8-Lip-HD (R8-Lip-HD-E) in the absence or the presence of the macropinocytosis inhibitor amiloride. The mean fluorescence (*MF*) of 10,000 cells was measured by flow cytometry and is expressed as the -fold increase in fluorescence measured for cells incubated with only R8-Lip-LD-RA. *Error bars* represent the ±S.D. for two different experiments performed in duplicate.

(36), did not show significant colocalization with both liposomes (data not shown). These results are consistent with the results of the inhibition study explained above, confirming the change of the cellular entry port upon changing the peptide density on the liposomal surface.

Stimulation of Macropinocytosis by R8-Lip—During the colocalization study between R8-Lip-HD and ND, we observed that the uptake of ND is increased significantly compared with cells treated with ND alone (data not shown). Using flow cytometry, we quantitatively confirmed the increase in the uptake of ND in the presence of R8-Lip-HD (supplemental Fig. S3). These results indicate that the R8-Lip-HD may have the ability to stimulate uptake through macropinocytosis, and this might be the reason for the change in the major entrance route by the change in peptide density on the liposomal surface. To investigate this hypothesis, we incubated cells with fixed concentrations of R8-Lip-LD-containing rhodamine aqueous phase (R8-Lip-LD-RA) together with increasing amounts of empty R8-Lip-HD (R8-Lip-HD-E) and then measured the internalized R8-Lip-LD-RA using flow cytometry (Fig. 4). The presence of R8-Lip-HD-E increased the internalization of R8-Lip-LD-RA in a concentration-dependent manner. When a 5-fold excess of the R8-Lip-HD-E was used, a 6-fold increase in uptake of the R8-Lip-LD-RA was observed. Parallel experiments were performed in the presence of amiloride to inhibit internalization through macropinocytosis. The presence of amiloride almost completely inhibited the increase in uptake of R8-Lip-LD-RA at all concentrations used. These results indicate that R8-Lip-HD increased the uptake of R8-Lip-LD mainly through stimulating macropinocytosis, which suggests that a certain peptide concentration is required to stimulate uptake pathways that are different from the clathrin-mediated endocytosis.

Intracellular Fate of Different R8-Lip—Because R8-Lip modified with different densities of R8 peptide follow different uptake pathways as suggested earlier, we investigated the intracellular fate of the liposomes in both cases using confocal laser scanning microscopy. We incubated cells with R8-Lip-LD or R8-Lip-HD, both of which contained an aqueous rhodamine phase, for 30 min, after which, the medium was exchanged with liposome-free medium, and the incubation was continued for a total of 1, 3, or 6 h. At the end of the incubation, the cells were examined by confocal microscopy, in which cells were scanned from bottom to top, and the section with the highest intracellular fluorescence possible was recorded for each cell (representative images are shown in supplemental Fig. S3). The pixel areas of the intracellular fluorescence in images from at least 15 different cells were quantified as described earlier. As shown in Fig. 5*A*, total intracellular fluorescence detected in the case of R8-Lip-LD after 1 h was reduced by >80% after 6 h, whereas it was only reduced by 25% in the case of R8-Lip-HD. Intracellular liposomes in the case of R8-Lip-LD are probably subjected to extensive degradation in the lysosomal compartment leading to the disappearance of most of the internalized fluorescence. Uptake by mac-

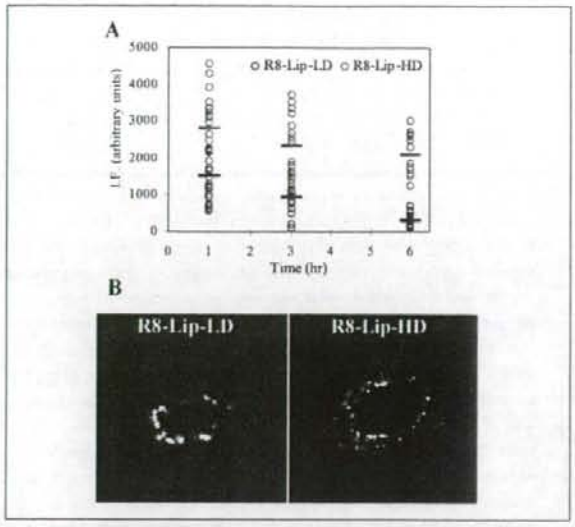

FIGURE 5. **Intracellular fate of different R8-Lip and colocalization with lysosomes.** *A*, a quantitative analysis of intracellular fluorescence. Cells were incubated with R8-Lip-LD (*blue circles*) or R8-Lip-HD (*red circles*) for 30 min, and then the medium was changed to liposome-free medium and incubation continued for a total of 1, 3, or 6 h before observation with confocal microscopy. Pixel areas of intracellular fluorescence (*I.F.*) from 15 cells were determined in each case as described under "Experimental Procedures." *Blue* and *red short lines* indicate the average fluorescence in each case. *B*, representative images of NIH3T3 cells treated with R8-Lip-LD or R8-Lip-HD containing rhodamine aqueous phase at 37 °C for 30 min then incubated in fresh liposome-free medium for a total of 3 h and subsequently observed by confocal microscopy. The lysosomes were stained green with LysoSensor before observation.

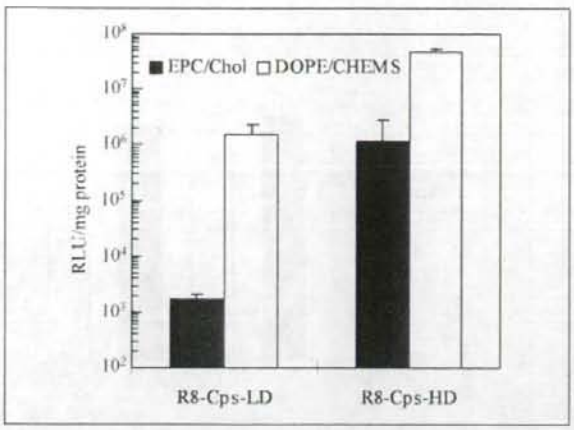

FIGURE 6. **Comparison of transfection activities of different DNA-coated particles.** A luciferase coding DNA-coated particles modified with low density (R8-Cps-LD) or high density (R8-Cps-HD) of R8 were prepared with a lipid envelope containing EPC/Chol or DOPE/CHEMS and used to transfect cells. Luciferase activities were measured as described under "Experimental Procedures" 24 h after transfection and are expressed as the relative light unit (*RLU*) per milligram of protein. Data represent the mean and ± S.D. of three different experiments performed in triplicate.

ropinocytosis involves the formation of large heterogeneous macropinosomes (>1 μm), which have been proposed to be leaky (33). The intracellular fate of macropinosomes differs depending on the cell type (32). In macrophages, they tend to completely merge with lysosomes, whereas in other cell types, they fuse only with other macropinosomes and tend to be recycled and their contents are not targeted for lysosomal degradation (32). To investigate the colocalization with lysosomes, we incubated cells with different R8-liposomes for 30 min followed by incubation in liposome-free medium for 2.5 h, and then we stained the lysosomal compartment with FITC LysoSensor before observation by confocal microscopy (Fig. 5*B*). A high degree of colocalization between R8-Lip and lysosomal compartment was found in the case of R8-Lip-LD that were internalized mainly by clathrin-mediated endocytosis, whereas only a partial colocalization could be found in the case of R8-Lip-HD. This indicates that internalization through macropinocytosis may represent a good tool for avoiding lysosomal degradation. Therefore, the R8-Lip-HD is less subject to lysosomal degradation, which may explain why high levels of intracellular fluorescence could be observed in this case even after 6 h.

To further confirm these findings, we examined the fate of R8-Lip-LD-RA that had been internalized in the absence or the presence of R8-Lip-HD-E to stimulate macropinocytosis. In the absence of R8-Lip-HD-E (*i.e.* clathrin-mediated endocytosis being the major entrance pathway), the intracellular fluorescence observed after 1 h mostly disappeared after 6 h (data not shown). Under the same conditions but in the presence of R8-Lip-HD-E (*i.e.* macropinocytosis is the major entrance pathway), high levels of intracellular fluorescence were found, even after 6 h (representative images are shown in supplemental Fig. S3). This confirms that particles internalized by macropinocytosis are less subject to lysosomal degradation and that the presence of R8-Lip-HD changes the intracellular trafficking and the fate of the R8-Lip-LD.

Enhanced Transfection Activities of R8-Cps Using Fusiogenic Lipids—The data presented above suggest that particles internalized by macropinocytosis (*i.e.* R8-Cps-HD) are not highly subject to lysosomal degradation compared with those internalized through clathrin-mediated endocytosis (*i.e.* R8-Cps-LD). Therefore, the difference in gene expression observed in Fig. 1*C* seems to arise mainly from the ability of both particles to avoid lysosomal degradation. To further assess the ability of different R8-Cps to escape from endosomes or lysosomes, we examined the effect of the fusiogenic lipid dioleoylphosphatidylethanolamine (DOPE), which has the ability to enhance the endosomal escape of particles trapped in endosomal vesicles through fusion with the endosomal membrane (37). We prepared and tested the transfection activities of R8-Cps consisting of a lipid envelope prepared with the non-fusiogenic lipids EPC and Chol or with the fusiogenic lipid DOPE and cholesteryl hemisuccinate (CHEMS) (37, 38). In the presence of DOPE, the transfection activities of R8-Cps-LD were increased by about 3 orders of magnitude, whereas transfection activities of R8-Cps-HD were increased by less than 2 orders of magnitude (Fig. 6). This indicates that the low transfection activities in the case of non-fusiogenic R8-Cps-LD is not due to the low cellular uptake, but mainly due to the low endosomal escape ability. The enhanced activities of the fusiogenic R8-Cps-HD may occur due to the enhanced endosomal escape of the fraction of the particles, which was internalized by clathrin-mediated endocytosis. Another possibility is that the fusiogenic lipid can further enhance the release of the particles from macropinosomes. In either case, the presence of devices that can enhance endosomal escape appears to be useful in terms of increasing the transfection activities of particles modified with the R8 peptide. Using confocal microscopy, we confirmed that macropinocytosis is the major entrance pathway for R8-Cps-HD and that the lipid composition had no effect on the internalization mechanism (data not shown).

Contribution of Different Uptake Pathways in Gene Expression—Because macropinocytosis is the major contributor to the uptake of R8-Cps-HD, whereas clathrin-mediated uptake is a relatively minor one, we investigated the contribution of both pathways in the gene expression process mediated by R8-Cps-HD (DOPE/CHEMS) (Fig. 7). A minor inhibition of gene expression was observed after blocking

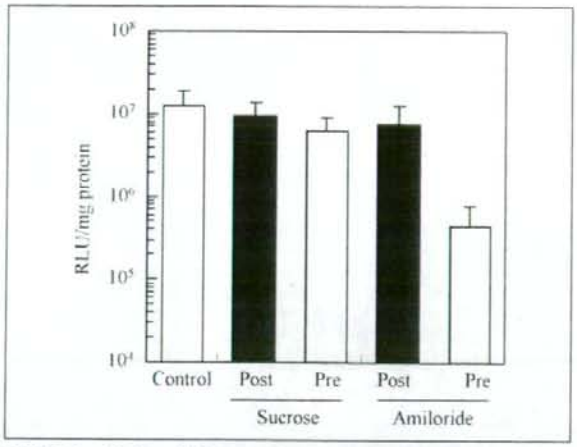

FIGURE 7. **Contribution of different uptake pathways in gene expression.** Cells were transfected with R8-Cps-HD (lipid envelope consisting of DOPE/CHEMS) in the absence (*Control*) or the presence (*Pre*) of sucrose or amiloride as described under "Experimental Procedures." To control the effects of sucrose and amiloride on intracellular events, cells were first loaded with R8-Cps-HD then treated with these reagents (*Post*). Luciferase activities were measured 12 h after transfection and are expressed as the relative light unit (*RLU*) per milligram of protein. Data represent the mean and ±S.D. of three different experiments performed in triplicate.

internalization through clathrin-mediated endocytosis using a hypertonic medium. This shows that the minor fraction that is internalized through this pathway does not actually lead to efficient gene expression. Meanwhile, blocking internalization through macropinocytosis caused a strong inhibition in gene expression (~95%), confirming that this pathway is the major contributor to efficient gene expression, in accordance with the above findings. Therefore, the role of R8 in increasing gene expression levels is not only increasing the binding to the cell surface, but extends to changing the uptake mechanism to more efficient pathways and the subsequent control of the intracellular trafficking of the particles.

DISCUSSION

PTDs like TAT and other arginine-rich peptides have been used to promote the cellular delivery of many types of cargos (1–3). Similarly, the R8 peptide was shown to be efficiently internalized into cells and to be able to mediate the cellular delivery of macromolecules, including peptides, proteins, and plasmid DNA (19, 39). However, the uptake mechanism of the arginine-rich peptides and their cargos is a matter of intense discussion in the literature. Different reports have demonstrated the involvement of different endocytic pathways in the uptake of these peptides or their cargos (11–18). This discrepancy of results suggests that some factors may affect the internalization mechanism, such as the properties of the peptide and cargos and the linkage between them. One factor that can possibly affect the internalization mechanism is the peptide concentration on the cargo surface. In this study, we investigated the uptake mechanisms of liposomes modified with the R8 peptide, and we focused on how the peptide density on the liposome surface affects the internalization mechanism. Furthermore, we followed the intracellular trafficking of internalized liposomes to understand the environment they are in and to rationally improve the system to achieve maximum activity.

We prepared R8-modified liposomes using a simple procedure in which the peptide is attached to a stearyl moiety that acts as an anchor to the lipid membrane of the liposomes. To examine the integrity of the liposomes during internalization, we examined the uptake of double-labeled R8-liposomes modified with different densities of the peptide (R8-Lip-LD and R8-Lip-HD). Cells treated with different R8-Lip for 1 h showed a high intracellular fluorescence, and both liposomal labels were colocalized on the plasma membrane or in the cytosol of cells in both cases (supplemental Fig. S1). The intracellular colocalization of the markers excludes the possibility of fusion between the liposomal membrane and the cell membrane. In addition, the intracellular fluorescence in both cases appeared as punctuated signals in the cytosol indicating a possible contribution of endocytosis, a finding that is further supported by the strong inhibition of uptake after energy depletion (Fig. 2). This clearly supports recently reported data suggesting that endocytic uptake is essential for cellular uptake of particles modified with arginine-rich peptides (11–18). Similar results showing efficient cellular uptake of intact PTD-modified liposomes have been reported previously (4–6).

We initially obtained evidence that the role of R8 extends beyond just increasing the binding of the particles to the cell surface to changing the fate of internalized liposomes. R8-Cps modified with low R8 density were taken up by cells, however, did not produce significant gene expression. The R8-Cps modified with high R8 density produced a 3 orders of magnitude higher gene expression, whereas the internalized particles were less than one order of magnitude higher than the low density particles. This indicates that the intracellular fate of the particles is improved by increasing the peptide density. It is generally accepted that different uptake mechanisms lead to different intracellular trafficking of internalized particles, because the intracellular fate of particles is closely linked to the entry mode. We hypothesized that the uptake mechanism is a strong candidate for explaining this difference in the intracellular fate of the particles depending on the peptide density. Therefore, we investigated the contribution of different endocytic pathways to the internalization of the R8-Lip using flow cytometry after confirming that the measured fluorescence represented only internalized liposomes by removing the surface-bound liposomes with a heparin wash (12), and the results were confirmed using confocal microscopy of living cells. It was recently shown that the internalization of the TAT-Cre fusion protein as well as that of R8 and TAT peptides occurs mainly through macropinocytosis (14–16). Here, we show that large drug carriers, such as liposomes that are ~100 nm in diameter, can also be internalized by macropinocytosis. Evidence for this includes the strong inhibition of uptake in the presence of the macropinocytosis inhibitor, amiloride (Fig. 2), and the high colocalization with the macropinocytosis marker, neutral dextran (Fig. 3). Furthermore, we found that a high peptide density on the liposomal surface is required for internalization by this pathway, because the low density R8-Lip were internalized mainly by clathrin-mediated endocytosis. In addition, the presence of high density R8-Lip stimulated the macropinocytosis-mediated uptake of neutral dextran and the low density R8-Lip. Surprisingly, the presence of the same concentration of peptide, but in the free form, failed to stimulate the macropinocytosis-mediated uptake of low density R8-Lip and only slightly increased the uptake of the macropinocytosis marker (data not shown). Therefore, the extent of stimulation of macropinocytosis is significantly higher in the case of R8-Lip-HD than in the case of the free peptide. This suggests that the liposomal surface can provide regions in which R8 is highly condensed, thus enhancing interaction with the cell membrane, and this localized interaction might be required to stimulate macropinocytosis. It was previously shown that arginine-rich peptides are able to induce a significant rearrangement in the cell cytoskeleton similar to that seen during macropinocytosis (16). This rearrangement may be responsible for the stimulation of uptake through macropinocytosis, which is shown here.

The uptake of condensed DNA particles coated with a lipid envelope

modified with high R8 density occurs also by macropinocytosis (data not shown). However, we previously reported that the uptake of complexes formed directly between R8 and DNA are mainly internalized by clathrin-mediated endocytosis (22) and are mainly trapped in the endosomes (40). This difference between direct complexation and lipid coating indicates that the nature of the interaction between the peptide and the cell surface is important in stimulating macropinocytosis. This also demonstrates the importance of the lipid envelope in controlling the topology of the peptide to determine the entrance route, because the ability to stimulate macropinocytosis is higher for the R8 peptide on the liposome surface compared with the R8 complexed with DNA.

One of the important issues is the difference in intracellular trafficking after clathrin-mediated endocytosis and macropinocytosis that can be stimulated by a high density of the R8 peptide on liposomal surface. The normal endosomes formed after clathrin-mediated endocytosis eventually fuse with lysosomes where degradation of the internalized material occurs, whereas the fate of the macropinosomes depends on the cell type. For example, in macrophages, they fuse with lysosomes while they are mainly recycled and are not efficiently targeted for lysosomal degradation in some other cell types (32). The low extent of colocalization between R8-Lip-HD and lysosomes (Fig. 5*B*) suggests that macropinosomes in the cell line used here are not targeted for lysosomal degradation. We show here that macropinocytosis is more favorable than the clathrin-mediated endocytosis in terms of gene expression, because blocking internalization through macropinocytosis caused a ~95% inhibition in gene expression. The data presented here suggest that the superiority of macropinocytosis is mainly due to the low level of lysosomal degradation of internalized particles, indicating the significance of macropinocytosis as an entrance pathway. In addition, the internalized particles may be easily released to the cytosol, because macropinosomes are assumed to be leaky compared with other endocytic vesicles (33). This ability appears to be enhanced by the use of pH-sensitive fusiogenic lipids, such as DOPE (Fig. 6).

Similar to previous reports using other PTDs (27, 28), the presence of heparin in the medium dramatically inhibited the cellular binding and uptake of R8-modified particles, suggesting that the presence of cell-surface HSPGs may be important for cellular binding. Based on the previous finding that arginine-rich peptides induce cytoskeleton rearrangement (16), and our finding that a high peptide density is required to stimulate macropinocytosis, we speculate that a strong and multiple binding between the R8 peptide and the cell-surface HSPGs may be required to affect the latter in a way that would induce a cytoskeleton rearrangement resulting in the initiation of raffle formation followed by uptake via macropinocytosis. Such a proposed multiple binding is available only in the case of the high density R8-Lip. Although the exact role of cell-surface HSPGs in cellular uptake is not clear, their cytoplasmic domains are known to interact with the actin cytoskeleton (41), which suggests that surface proteoglycans may be involved in stimulating endocytic uptake. A significant role for proteoglycans in the phagocytosis of cationic vectors was previously reported (42).

In conclusion, our results show that the density of the R8 peptide determines the internalization mechanism, which is directly linked to intracellular trafficking. The remarkable difference in gene expression between DNA-coated particles modified with different R8 densities can be explained principally by differences in the intracellular trafficking of DNA as well as the carriers. Our results indicate that cells have the ability to recognize differences in the nature of nanoparticles and to respond by internalizing them via different mechanisms.

Acknowledgment—We thank Dr. M. S. Feather for his helpful advice in writing the English manuscript.

REFERENCES

1. Schwarze, S. R., Hruska, K. A., and Dowdy, S. F. (2000) *Trends Cell Biol.* **10,** 290–295
2. Lindgren, M., Hallbrink, M., Prochiantz, A., and Langel, U. (2000) *Trends Pharmacol Sci.* **21,** 99–103
3. Snyder, E. L., and Dowdy, S. F. (2004) *Pharm. Res.* **21,** 389–393
4. Torchilin, V. P., Rammohan, R., Weissig, V., and Levchenko, T. S. (2001) *Proc. Natl. Acad. Sci. U. S. A.* **98,** 8786–8791
5. Fretz, M. M., Koning, G. A., Mastrobattista, E., Jiskoot, W., and Storm, G. (2004) *Biochim. Biophys. Acta* **1665,** 48–56
6. Marty, C., Meylan, C., Schott, H., Ballmer-Hofer, K., and Schwendener, R. A. (2004) *Cell Mol. Life Sci.* **61,** 1785–1794
7. Torchilin, V. P., Levchenko, T. S., Rammohan, R., Volodina, N., Papahadjopoulos-Sternberg, B., and D'Souza, G. G. (2003) *Proc. Natl. Acad. Sci. U. S. A.* **100,** 1972–1977
8. Vives, E., Brodin, P., and Lebleu, B. (1997) *J. Biol. Chem.* **272,** 16010–16017
9. Derossi, D., Calvet, S., Trembleau, A., Brunissen, A., Chassaing, G., and Prochiantz, A. (1996) *J. Biol. Chem.* **271,** 18188–18193
10. Trehin, R., and Merkle, H. P. (2004) *Eur. J. Pharm. Biopharm.* **58,** 209–223
11. Richard, J. P., Melikov, K., Vives, E., Ramos, C., Verbeure, B., Gait, M. J., Chernomordik, L. V., and Lebleu, B. (2003) *J. Biol. Chem.* **278,** 585–590
12. Lundberg, M., Wikstrom, S., and Johansson, M. (2003) *Mol. Ther.* **8,** 143–150
13. Drin, G., Cottin, S., Blanc, E., Rees, A. R., and Temsamani, J. (2003) *J. Biol. Chem.* **278,** 31192–31201
14. Wadia, J. S., Stan, R. V., and Dowdy, S. F. (2004) *Nat. Med.* **10,** 310–315
15. Kaplan, I. M., Wadia, J. S., and Dowdy, S. F. (2005) *J. Control. Release* **102,** 247–253
16. Nakase, I., Niwa, M., Takeuchi, T., Sonomura, K., Kawabata, N., Koike, Y., Takehashi, M., Tanaka, S., Ueda, K., Simpson, J. C., Jones, A. T., Sugiura, Y., and Futaki, S. (2004) *Mol. Ther.* **10,** 1011–1022
17. Fittipaldi, A., Ferrari, A., Zoppe, M., Arcangeli, C., Pellegrini, V., Beltram, F., and Giacca, M. (2003) *J. Biol. Chem.* **278,** 34141–34149
18. Ferrari, A., Pellegrini, V., Arcangeli, C., Fittipaldi, A., Giacca, M., and Beltram, F. (2003) *Mol. Ther.* **8,** 284–294
19. Futaki, S., Suzuki, T., Ohashi, W., Yagami, T., Tanaka, S., Ueda, K., and Sugiura, Y. (2001) *J. Biol. Chem.* **276,** 5836–5840
20. Suzuki, T., Futaki, S., Niwa, M., Tanaka, S., Ueda, K., and Sugiura, Y. (2002) *J. Biol. Chem.* **277,** 2437–2443
21. Brooks, H., Lebleu, B., and Vives, E. (2005) *Adv. Drug Deliv. Rev.* **57,** 559–577
22. Khalil, I. A., Futaki, S., Niwa, M., Baba, Y., Kaji, N., Kamiya, H., and Harashima, H. (2004) *Gene Ther.* **11,** 636–644
23. Schwarze, S. R., Ho, A., Vocero-Akbani, A., and Dowdy, S. F. (1999) *Science* **285,** 1569–1572
24. Eguchi, A., Akuta, T., Okuyama, H., Senda, T., Yokoi, H., Inokuchi, H., Fujita, S., Hayakawa, T., Takeda, K., Hasegawa, M., and Nakanishi, M. (2001) *J. Biol. Chem.* **276,** 26204–26210
25. Futaki, S., Ohashi, W., Suzuki, T., Niwa, M., Tanaka, S., Ueda, K., Harashima, H., and Sugiura, Y. (2001) *Bioconjug. Chem.* **12,** 1005–1011
26. Kogure, K., Moriguchi, R., Sasaki, K., Ueno, M., Futaki, S., and Harashima, H. (2004) *J. Control. Release* **98,** 317–323
27. Richard, J. P., Melikov, K., Brooks, H., Prevot, P., Lebleu, B., and Chernomordik, L. V. (2005) *J. Biol. Chem.* **280,** 15300–15306
28. Console, S., Marty, C., Garcia-Echeverria, C., Schwendener, R., and Ballmer-Hofer, K. (2003) *J. Biol. Chem.* **278,** 35109–35114
29. Almofti, M. R., Harashima, H., Shinohara, Y., Almofti, A., Baba, Y., and Kiwada, H. (2003) *Arch. Biochem. Biophys.* **410,** 246–253
30. Lamaze, C., and Schmid, S. L. (1995) *Curr. Opin. Cell Biol.* **7,** 573–580
31. Conner, S. D., and Schmid, S. L. (2003) *Nature* **422,** 37–44
32. Swanson, J. A., and Watts, C. (1995) *Trends Cell Biol.* **5,** 424–428
33. Meier, O., Boucke, K., Hammer, S. V., Keller, S., Stidwill, R. P., Hemmi, S., and Greber, U. F. (2002) *J. Cell Biol.* **158,** 1119–1131
34. Parton, R. G. (2003) *Nat. Rev. Mol. Cell Biol.* **4,** 162–167
35. Singh, M. (1999) *Curr. Pharm. Des.* **5,** 443–451
36. Zuhorn, I. S., Kalicharan, R., and Hoekstra, D. (2002) *J. Biol. Chem.* **277,** 18021–18028
37. Farhood, H., Serbina, N., and Huang, L. (1995) *Biochim. Biophys. Acta* **1235,** 289–295
38. Hafez, I. M., and Cullis, P. R. (2000) *Biochim. Biophys. Acta* **1463,** 107–114
39. Futaki, S. (2002) *Int. J. Pharm.* **245,** 1–7
40. Akita, H., Ito, R., Khalil, I. A., Futaki, S., and Harashima, H. (2004) *Mol. Ther.* **9,** 443–451
41. Yoneda, A., and Couchman, J. R. (2003) *Matrix Biol.* **22,** 25–33
42. Kopatz, I., Remy, J. S., and Behr, J. P. (2004) *J. Gene Med.* **6,** 769–776

IUBMB *Life*, 58(1): 1–6, January 2006

Taylor & Francis
Taylor & Francis Group

Critical Review

Engineered Bio-nanocapsules, the Selective Vector for Drug Delivery System

Dongwei Yu[1], Takayuki Fukuda[1,2], Tuoya[1], Shun'ichi Kuroda[3,6], Katsuyuki Tanizawa[3,6], Akihiko Kondo[4,6], Masakazu Ueda[5,6], Tadanori Yamada[6], Hiroko Tada[1] and Masaharu Seno[1,6,7]

[1]*Graduate School of Natural Science and Technology, Okayama University, 3.1.1 Tsushima-Naka, Okayama 700-8530, Japan*
[2]*MRP Division, Katayama Chemical Industries Co. Ltd., 2.5.10 Doshomachi, Chuo-ku, Osaka 541-0045, Japan*
[3]*Institute of Scientific and Industrial Research, Osaka University, 8.1 Mihogaoka, Ibaraki, Osaka 567-0047, Japan*
[4]*Faculty of Engineering, Kobe University, 1.1 Rokkodai, Naka, Kobe, Hyogo 657-8501, Japan*
[5]*Keio University, School of Medicine, 35 Shinanomachi, Shinjuku-ku, Tokyo 160-8582, Japan*
[6]*Research Center, Beacle, Inc., Okayama Research Park Incubation Center, 5303 Haga, Okayama 701-1221, Japan*
[7]*Research Center for Biomedical Engineering, Okayama University, 3.1.1 Tsushima-Naka, Okayama 700-8530, Japan*

Summary

The bio-nanocapsule (BNC) is our concept of artificial hollow nanoparticles that have been designed and produced through biotechnological procedures. We proposed an empty virus-like particle, which consists of a recombinant L envelope protein of hepatitis B virus (HBV) and a lipid derived from the host cell, as an engineered BNC. Although this BNC was first developed as an immunogen of hepatitis B vaccine, the pre-S1 region in N-terminus of L envelope protein confers hepatocyte specific infectivity of HBV on the BNC. This recombinant BNC is now being developed as a novel platform of drug delivery system (DDS) vector for selective delivery.

IUBMB *Life*, 58: 1–6, 2006

Keywords Vector; specific infection; delivery; topology.

INTRODUCTION

The drug delivery system (DDS) is one of the areas of intense focus recently in pharmacology. However, the development of DDS technology has concentrated on the controlled release of pharmaceutical drugs encapsulated in a nano-sphere composed of such substances as micelles and liposomes. The targeting potential of the pinpoint delivery in DDS has appeared to be ignored since antibody-based 'missile therapy' has been extensively studied by immunologists. Although live viruses are sometimes toxic or oncogenic to the infected cells, they have been found to be extremely useful for the transfer of genes to the cells. Consequently, the development of artificial viruses as vectors for gene transduction or gene therapy has caused vigorous research worldwide as a part of nanobiotechnology. This new area of science deals with molecules as nanostructures and molecules in nanostructures such as nanoparticles not only for the conventional analyses of molecules but for the extensive development of new tools in biotechnology and medical engineering (*1*). In presenting an overview of the viruses, it may be noted that many of them are known to have host ranges, but to rarely exhibit cell type or tissue type selectivity. Only a few of them exhibit some narrow range of cell type selectivity like HBV or HIV, for example. The HBV is among the best known viral pathogens that affect humans. It has been studied for more than 60 years in the hope of learning how to prevent its infection. HBV is a small enveloped DNA virus of the hepadnaviridae family (*2, 3*). The surface proteins of the virion envelope are found to consist of three types of glycoproteins, which are called small- (S-), middle- (M-) and large- (L-) protein (*4*). These three different proteins, which are cotranslationally integrated into the rough endoplasmic reticulum as transmembrane proteins, are encoded in a single open reading frame of HBV genome with three independent, but in-frame, AUG translational start codons (*5, 6*). The HBV infected cells secrete, not only the complete 42-nm infectious virions, but also a large excess of 22-nm noninfectious empty envelope particles. The latter are composed of S-protein (*7–9*). Valenzuela et al. successfully prepared HBV surface antigens (HBsAg) as recombinant S-protein, which organized itself as a particle having a diameter of 22 nm (*10*). When produced in

Received 21 October 2005; accepted 20 November 2005
Address correspondence to: Masaharu Seno, Graduate School of Natural Science and Technology, Okayama University, 3.1.1 Tsushima-Naka, Okayama 700-8530, Japan. Tel/Fax: +81 86 251 8216.
E-mail: mseno@cc.okayama-u.ac.jp

ISSN 1521-6543 print/ISSN 1521-6551 online © 2006 IUBMB
DOI: 10.1080/15216540500484368

yeast, recombinant M- and L-proteins were also found to associate as hollow virus-like particles, although they had been only developed as immunogens for hepatitis B vaccines (*11, 12*). The virus-like particle composed of the recombinant L-proteins had a diameter of approximately 200 nm (*12, 13*). Due to the specific affinity to human hepatocytes localized in the amino-terminus of L-protein, only the nanometer size hollow particle, composed of L-proteins, showed extremely selective targeting potential as a novel type of DDS vector to be directed to the human liver (*14*). Because of its favorable potential, we have proposed a bio-nanocapsule (BNC) concept as an efficient nanomachine to achieve tissue-/cell-type specific delivery of genes, drugs and proteins.

PROPERTIES OF ENGINEERED BIO-NANOCAPSULES

Our BNC is described as a hollow protein nano-scale particle. Some viral core particles, which consist of sole self-organizing proteins, such as HBV core antigen (cAg) and others that also consist of self-organizing proteins with lipids as essential components, like the envelope of hemaglutinating virus of Japan (HVJ), are conceivable. Since the BNC should function as a capsule that contains some encapsulated foreign substances in its interior, the lipid component appears to be essential to confer flexibility in order to maintain a suitable shape as a DDS vector even after the physical implementation of encapsulation such as electroporation. In this context, HBV cAg does not appear to be suitable as a capsule due to the tight association of each component of cAg. The HBV envelope proteins form a BNC, since almost 80% of the components are L-, M- or S-proteins. This BNC of HBV can be formed by a single species of viral surface proteins. Therefore, newly engineered BNC can be designed and produced by modifying the protein in a variety of ways by a simple procedure. The L-protein is composed of three regions, the 108 or 119 amino acids (subtype ayw or adw, respectively) pre-S1 region (*8, 15*) involved in the direct recognition of human hepatocytes, the 55 amino acids pre-S2 region associated with the polymerized albumin-mediated interaction (*16*), and the major 226 amino acids S protein region.

When L-protein was expressed in yeast cells, it failed to assemble into a subviral particle, unlike S protein, although the protein is efficiently expressed (*17, 18*). The synthetic gene for chicken-lysozyme signal (C-SIG) peptide was fused at the 5′-terminal of L gene. The C-SIG peptide was processed correctly by the yeast secretory apparatus and led the pre-S1 region in traversing the ER membrane. Then, the L-proteins assembled themselves into a virus-like particle as a L-BNC. A small region of Ser^{44}–Thr^{48} containing a site sensitive to the trypsin-like protease (Arg^{48}–Thr^{49}) has been deleted from pre-S2. The addition of C-SIG peptide and deletion of Ser^{44}–Thr^{48} did not affect the stability of L-protein and polymerized human serum albumin binding activity (*19*).

This engineered L-protein, produced as a L-BNC in recombinant yeast cells, has been purified and characterized. The average molecular mass of a L-BNC was confirmed by equilibrium sedimentation to be 6.4×10^6, which indicates that about 110 molecules of L-protein associate to form an L-BNC. Atomic force microscopy in a moist atmosphere showed the L-BNCs to be spherical particles with diameters ranging from 50–500 nm and an average of 200 nm. The L-BNCs were stable at a high temperature of around 80°C and, for a week, at 4°C, but were found to become unstable as a result of freezing and thawing or treatment with dithiothreitol (*19*).

ENGINEERED BIO-NANOCAPSULE HAS THE SAME SPECIFIC INFECTIVITY AS HBV

HBV, a member of hepadnaviridae, known as a family of hepatotropic, has a very narrow host-range and is limited to infecting naturally humans and some higher primates, such as the chimpanzee (*11, 20, 21*). It has been demonstrated that the L-protein is important in forming an infectious virus particle and essential for receptor interaction (*22–24*). In particular, the 108 or 119 amino acids of pre-S1 domain of glycosylated L-protein have long been considered to be responsible for receptor binding and the host range (*22, 25, 26*), while the 55 amino acids of pre-S2 is dispensable for viral infectivity (*27*). The involvement of L-protein in the infection stage has been confirmed. Furthermore, the segment from 21 to 47 amino acid of pre-S1 was found to be indispensable for HBV infection (*28–31*). However, the latest research demonstrated that more amino acid residues, extending from 3 to 77, are involved in this process (*22*). The pre-S1 region of the L-protein, displayed on the surface as the specific ligand for receptor of human hepatocytes, certainly confers on the L-BNC the high infectivity to hepatocytes limited to humans and primates. Very recently, we have shown that the L-BNC efficiently delivers the gene for green fluorescence protein (GFP) and GFP protein to human liver cells in a cell type specific manner *in vitro* and *in vivo* (*14, 32*). Thus, our engineered L-BNC was demonstrated to be an efficient delivery mimicking HBV.

ENGINEERED BIO-NANOCAPSULE CAN DELIVER SUBSTANCES TO TARGET TISSUE OR CELL

HBV is the only DNA virus that targets the liver where it efficiently infects hepatocytes. This ability permits the development of an HBV-based vector for liver-directed gene transfer with foreign DNA inserted into the virus genome (*33, 34*). However, this viral vector is not suitable for the delivery of substances other than DNA. Since the L-BNC is an empty particle that recognizes human hepatocytes just like HBV, electroporation was used to encapsulate the DNA and small chemical compounds that were inside the L-BNC (*14*). The GFP gene or fluorescent chromophore calcein was successfully encapsulated by electroporation and transferred